UNIVERSITÀ DEGLI STUDI DI PADOVA

Sede Amministrativa: Università degli Studi di Padova

Dipartimento di Istologia, Microbiologia e Biotecnologie Mediche

Scuola di Dottorato in Biochimica e Biotecnologie

Indirizzo Biotecnologie

Ciclo XXI

Role of TGFβ and mutant-p53 in metastasis control

Direttore della Scuola: Ch.mo Prof. Giuseppe Zanotti

Supervisore**:** Ch.mo Prof. Stefano Piccolo

Dottorando: Dr. Marco Montagner

INDEX

ABSTRACT

TGFβ ligands act as tumor suppressors in early stage tumors but are paradoxically diverted into potent prometastatic factors in advanced cancers. The molecular nature of this switch remains enigmatic. Here we show the workings of a previously undescribed pathway by which TGFβ fosters cell migration, invasion and metastasis. We found that TGFβ, together with oncogenic Ras and mutant-p53, but notably neither of these factors alone, is required for the assembly of a mutant-p53/Smad biochemical complex that binds p63, antagonizing its antimetastatic properties. *In vitro*, mutant-p53 is required to empower TGFβ-dependent invasion and migration and p63 is epistatic for these effects. Mechanically, Smad proteins bridge mutant-p53 to p63, allowing the former to inhibit the DNA binding of the latter, blocking the transcriptional activation of its downstream targets. *In vivo*, loss-of-mutant-p53, or gain-of p63, disables TGFβ-driven metastatic spread. Conversely, inhibition of p63 transforms noninvasive cells into motile-invasive cells. By transcriptomic analyses, functional validation and clinical verification we found two novel candidate metastasis suppressor genes downstream of this pathway associated with metastasis risk in a large cohort of breast cancer patients. Together, these results support a model in which the combination of two common oncogenic lesions, mutant-p53 and Ras, selected in early neoplasms to promote growth and survival, also prefigure a cellular set-up with particular metastasis proclivity. This trait can be exploited later during progression to drive a metastatic switch, once cells gain access to high levels of TGFβ, either autonomously produced or extracted from the microenvironment.

ABSTRACT (ITALIANO)

I ligandi della famiglia TGFβ agiscono come oncosoppressori nei primi stadi della tumorigenesi, ma paradossalmente sono mutati in fattori prometastatici nei tumori avanzati. La natura molecolare di questo cambiamento rimane enigmatica. In questo lavoro presentiamo il funzionamento di una via di segnale mai caratterizzata attraverso cui TGFβ stimola la migrazione cellulare, l'invasione tumorale e la metastasi. Abbiamo scoperto che TGFβ, assieme a p53 mutante e ad un'attivazione aberrante di Ras, è richiesto per l'assemblamento di un complesso biochimico p53-mutante/Smad, che lega p63, antagonizzando la sua attività anti-metastatica. Questo fenomeno non si osserva con nessuno dei tre fattori singolarmente. In vitro, p53 mutante è richiesta per permettere una migrazione cellulare indotta da TGFβ e p63 è epistatica a questo effetto. Meccanicisticamente, le proteine Smad fanno da ponte tra p53 mutante e p63, consentendo alla prima di bloccare il dominio di interazione al DNA della seconda, inibendo in questo modo l'attivazione trascrizionale dei geni bersaglio. In vivo, la perdita di p53 mutante, o l'acquisto di p63, disattivano la diffusione metastatica promossa da TGFβ. Dall'altra parte, l'inibizione di p63 trasforma cellule non invasive in invasive. Per mezzo di analisi del trascrittoma, validazione funzionale e clinica abbiamo scoperto due nuovi geni soppressori delle metastasi che agiscono a valle di questa cascata di eventi e che sono associati a rischio di metastasi in una significativa coorte di pazienti con cancro alla mammella. Sommati, questi risultati supportano un modello in cui la combinazione di due lesioni oncogeniche frequenti, p53 mutante e Ras, selezionate negli stadi precoci dei tumori per promuovere la sopravvivenza e la crescita, favoriscano uno scenario con una particolare tendenza alla metastasi. Questo tratto può essere sfruttato durante successivamente durante la progressione tumorale per indurre un comportamento metastatico, una volta che le cellule entrano in contatto con alti livelli di TGFβ prodotto autonomamente o dall'ambiente circostante.

PUBLICATIONS

Cordenonsi, M., **Montagner, M**., Adorno, M., Zacchigna, L., Martello, G., Mamidi, A., Soligo, S., Dupont, S., and Piccolo, S. (2007). Integration of TGF-beta and Ras/MAPK signaling through p53 phosphorylation. Science 315, 840-843.

Dupont, S., Mamidi, A., Cordenonsi, M., **Montagner, M**., Zacchigna, L., Adorno, M., Martello, G., Stinchfield, M.J., Soligo, S., Morsut, L., et al. (2009). FAM/USP9x, a deubiquitinating enzyme essential for TGFbeta signaling, controls Smad4 monoubiquitination. Cell 136, 123-135.

Martello, G., Zacchigna, L., Inui, M., **Montagner, M**., Adorno, M., Mamidi, A., Morsut, L., Soligo, S., Tran, U., Dupont, S., Cordenonsi, M., Wessely, O., Piccolo, S. (2007). MicroRNA control of Nodal signaling. Nature 449, 183-188.

Adorno, M., Cordenonsi, M., **Montagner, M**., Wang, C., Solari, A., Bobisse, S., Parenti, A., Rosato, A., Bicciato, S., Balmain, A., Piccolo, S. (2009) Cell, accepted for publication.

This was realized with the main contributions from the colleagues Dr.ssa Maddalena Adorno and Dr. Michelangelo Cordenonsi. I primarily contributed to the biochemistry and gene expression studies, both in vitro and in vivo. Dr. Antonio Rosato carried out the in vivo studies in nude mice and Prof. Anna Parenti helped with the histological characterization of tumor samples. Dr. Vincenzo Bronte and Dr. Silvio Bicciato were crucial for the microarray set-up and corresponding bioinformatic analysis, respectively. Finally, through the collaboration with Prof. Allan Balmain (UCSF) we had access to genetically matched mouse skin cell lines; the Balmain group provided us the data on p63 expression and function in squamous cell carcinomas.

INTRODUCTION

The TGFβ signaling cascade.

Cell behaviour relies on informational networks in which extracellular signal are transduced to the nucleus to be integrated into coherent genetic programs. A prominent role in this networks is played by the Transforming Growth Factor-β family of cytokines (TGFβ). TGFβ controls a variety of cellular responses from body axis formation, left-right patterning and organogenesis in the embryo to tumor suppression, immune surveillance, cellular homeostasis and differentiation in adult tissues. Loss of this control contributes to cancer, metastasis, fibrosis and several other diseases (Derynck et al., 2001; Massague, 2000; Wakefield and Roberts, 2002).

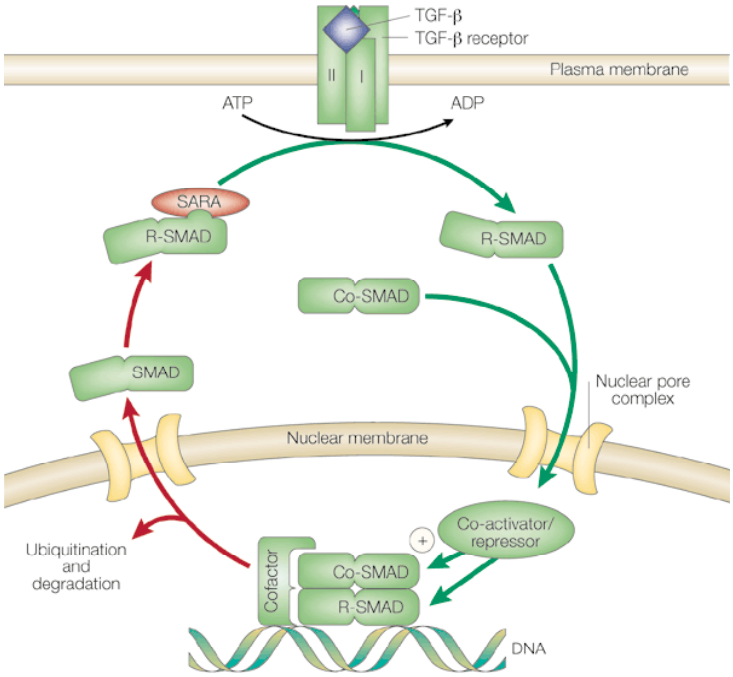

Nature Reviews | Molecular Cell Biology

The TGFβ family consist of more than 40 members that can be divided into two main branches: one comprises TGFβs, Activins, Leftys and Nodals, while the other is made of BMP ligands and Anti-Mullerian hormone. The signaling pathway of the TGFβ family, from the ligands to the target genes is well estabilished. The secreted, latent, precursor is cleaved by enzymes, such as furins, and the bioactive cytokine forms a dimer that bridges together two pairs of receptor serine-threonine kinases, known as Type I and Type II receptors. Each ligand of the TGFβ family binds to a specific Type I/Type II receptor couple; the main function of Type II Receptor is to activate Type I Receptor, which in turn activates Receptor-Smads proteins through phospholylation in the C-terminal domain. Activated R-Smads form a complex with Smad4, common to all R-Smads, and shuttles to the nucleus where they can activate or repress their target genes.

TGFβ regulates the expression of hundreds of genes by binding to their consensus target elements on DNA (CAGAC). However, the affinity of Smad interaction is typically quite low to be effective byitself; indeed, Smads requires additional cofactors to achieve effective binding to target genes' promoter. As each cell displays a particular set of Smad transcriptional partners, this mechanisms provide a first layer of control for differential gene expression attained by Smad.

TGFβ in tumor suppression and metastasis: a double edged sword.

The TGFβ cascade plays both positive and negative roles on tumorigenesis (Derynck et al., 2001; Wakefield and Roberts, 2002).

TGFβ is a potent inhibitor of proliferation in epithelial cells and other cell types and is considered a main tumor suppressor in normal tissues and in early stage neoplasms (Siegel and Massague, 2003). TGFβ inhibits progression of cell cycle by blocking it at late G1 phase with two main mechanisms: the induction of Cyclin Dependent Kinase inhibitors (Cdk-inhibitors) and repression of c-Myc. In epithelial cells, TGFβ induces the expression of p15, an inhibitor of cyclinD/CdK4-6 complex, and p21 which in turn blocks cyclinE/CdK2 complex. These effects are enhanced by Myc-repression, that is known for inducing cyclin D and inhibiting p21 and p15.

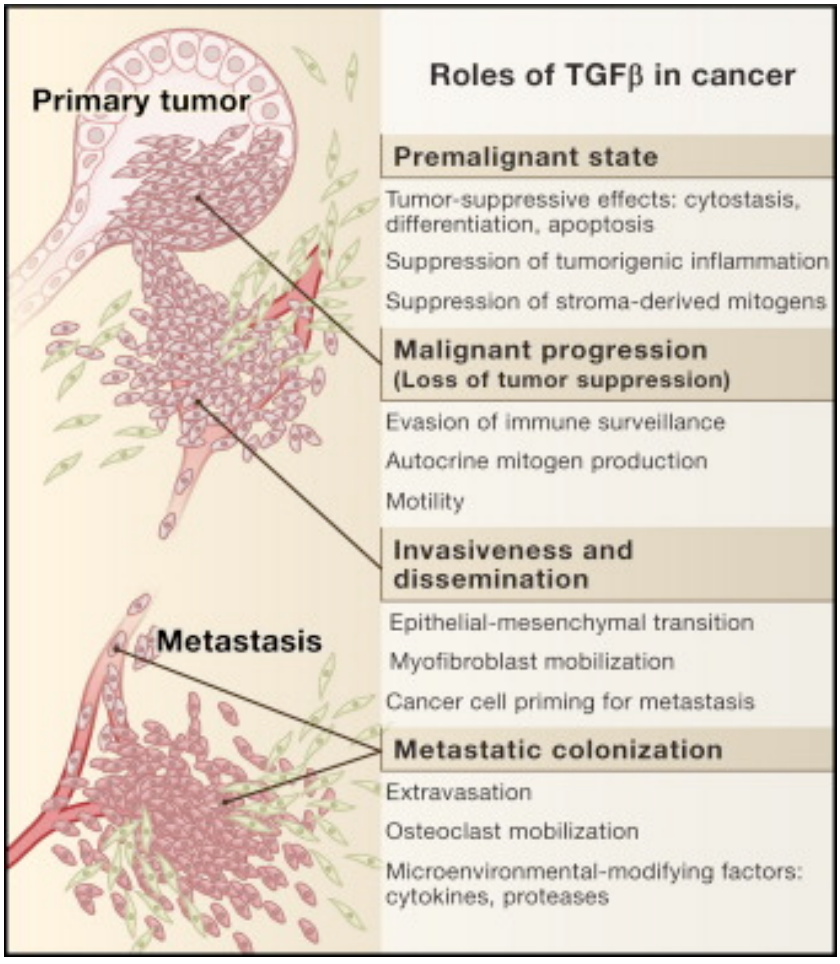

Loss of TGFβ tumor suppression is a hallmark of cancer. Yet, this is only rarely attained by mutations hitting the core pathway components. In contrast, it is well established that several TGFβ

responses remain fully operational in cancer cells and contribute positively to tumor invasiveness and metastasis (Derynck et al., 2001; Wakefield and Roberts, 2002). Metastasis is the cause of 90% of death from solid tumors; yet, the complexity of this process remains enigmatic. Several recent developments underlie, however, that for deeper understandings and clinical improvements it is mandatory to unveil, in mechanistic terms, the genetic and epigenetic changes that program the acquisition of distinct metastatic traits. These include the gain of invasive properties (i.e., loss of epitheliality, increased motility) and the bypass of the natural barriers normally preserving tissue architecture and function (i.e., degradation of basement membranes or extracellular matrix, and evasion from immune surveillance). In the second step, intravasation, tumor cells penetrate through the endothelium of blood and lymphatic vessels; only few cells survive in the circulation and manage to carry out the third step, extravasation, and enter into a distant site. Disseminated tumor cells typically remain dormant until a tiny subset of malignant cells carrying distinct profiles of genetic abnormalities are finally selected for their ability to grow in the new soil, generating secondary tumors (Fidler, 2003; Gupta and Massague, 2006).

p53 as Smad cofactor.

As outlined above, the output of TGFβ stimulation strongly depends on its cooperation with other proteins, such as Smad cofactors, and signaling cascades. Our group provided evidences that p53 family members are critical determinants for key TGFβ gene responses in different cellular and developmental settings. Indeed several TGFβ target genes in mammalian cells and *Xenopus* embryos are under joint-control of p53 and Smad (Cordenonsi et al., 2003). Mechanistically, the cooperation between p53 and Smads is attained by their direct physical interaction at the level of TGFβ target promoters. Of note, the simple physical interaction is not sufficient, but p53 and the activated Smad complex must be recruited at distinct *cis*-regulatory elements of a common target promoter, leading to synergistic activation of transcription. In mammalian cells, the biological relevance of the p53/Smad cooperation was investigated in the context of TGFβ growth arrest program such as the induction of the cdk-inhibitors p21 and p15.

p53 is a well-established sensor, as multiple cellular inputs converge on p53, mainly by triggering p53 post-transcriptional modification. We found that FGF/Ras pathway primes and activates p53 toward Smad cooperation for frog mesoderm development and mammalian cytostasis. Ras operates through CK1δ/ε, inducing p53 serine 6 and 9 phosphorylation in response to FGF/Ras/MAPK signaling. This result is in line with the role of autocrine TGFβ signaling in the proliferative arrest and senescence triggered by Ras activation (Vijayachandra et al., 2003) and the role of Ras as enhancer of growth suppression in epithelial cells, where it requires wild-type p53 (Ferbeyre and Lowe, 2002 ; Lowe et al., 2004 ; Lowe and Sherr, 2003).

Mutant-p53 and metastasis

p53 is one of the genes most frequently mutated in cancer cells. More that 80% of p53 mutations in cancers are missense mutations, generating stable, but transcriptionally deficient proteins (Soussi and Lozano, 2005). It is believed that the potential advantages for the tumor to retain a mutated p53, instead of deleting it for good, stem from molecularly undefined "gain-of-function" properties that render mutant-p53 a dominant oncogene.

Whether this entails the intersection with other pathways involved in neoplastic transformation is unknown. It has been proposed that the functions of mutant-p53 are not entirely neomorphic but may derive from corruptions - or mockery - of normal wild-type p53 properties (Cordenonsi et al., 2003). The involvement of mutant-p53 in cellular events that leads to transformation has been previously hypothesized on the basis of several evidences. For example, Li-Fraumeni patients, carrying germ-line p53 mutations, develop aggressive cancers at early age (Kleihues et al., 1997); moreover, breast and colon cancers carrying p53 mutations have been associated to a poorer prognosis than tumors lacking p53 expression (Soussi and Lozano, 2005); crucially, knock-in mice expressing mutant-p53 alleles from its natural promoter develop carcinomas metastasizing to various organs with high frequency, a phenotype rarely seen in mice with a p53-null allele (Hingorani et al., 2005; Lang et al., 2004; Olive et al., 2004)

Intriguingly, activating mutations in the Ras signaling pathway appear critical for the malignant phenotypes of mutant-p53 (Caulin et al., 2007; Hingorani et al., 2005; Li et al., 1997). Thus, p53 mutation, in concert with oncogenic Ras, leads to a gain of molecularly undefined properties that render mutant-p53 a dominant prometastatic factor.

We hypothesized that, just like wild-type p53 interacts with TGFβ and physiological Ras activation in growth control, also mutant-p53 might cooperate with the same pathways, but this time to trigger malignant cell behaviors. In other words, expression of mutant-p53, in the same step, would not only inactivate TGFβ tumor suppression, but also divert the cellular interpretation of TGFβ, transforming it into a metastatic factor with the help of oncogenic Ras signaling.

RESULTS

Mutant-p53, but not wild-type p53, bestows TGFβ -driven migratory phenotype on cells.

We sought to compare the effect of wild-type and mutant-p53 on the cellular response to TGFβ, both oncosuppressive and pro-oncogenic (Figure 1A). To this end, we took advantage of a lung cancer cell line, H1299, that carries an homozygous deletion of TP53 gene; in this way we could reconstitute the cell line either with p53-wild-type or the hot-spot p53H175R allele, whose expression can be induced from a ponasteron-inducible promoter. This inducible experimental design was set to avoid potential confounding effects caused by the genomic instability typically associated with constitutive expression of mutant-p53 (Soussi and Lozano, 2005). As shown in Figure 1B, wild-type and p53H175R are expressed at similar levels as measured by western blotting of lysates from ponasteron-treated cells. Of note, parental, wild-type and mutant-p53-expressing cells retained similar responsiveness to TGFβ, as established by two evidences: first, lysates of cultures treated with doses of TGFβ for 30 minutes displayed similar inductions of P-Smad3 (Fig. 1B); second, the ability of TGFβ to activate transcription from a transfected synthetic reporter of Smad activity (pCAGA12-lux) was comparable in parental and wild-type/mutant-p53-expressing cells (Fig. 1F). On the other side TGFβ treatment doesn't influence the level of p53 expressed protein (Fig. 1B), meaning that both isoforms of p53 and TGFβ are not regulating neither reciprocal stability nor activity.

In agreement with previous findings, reconstitution of H1299 cells with wild-type p53 rescued the ability of TGFβ to induce $p21^{WAF1}$, a hallmark gene of Smad cytostatic response (Figure 1B). In contrast, reconstitution with mutant-p53 was ineffective in this respect (Figure 1B). Strikingly, however, TGFβ treatment of p53H175R-H1299 cells caused them to shed their cuboidal epithelial shape and acquire instead a more mesenchymal phenotype, characterized by number of dynamic protrusions, such as filopodia and lamellipodia (Fig. 1C). These were not present in parental cells or in cells reconstituted with wild-type p53 (Fig. 1C and data not shown). These results suggest that concomitant activity of TGFβ/Smad and mutant-p53 expression causes cytoskeletal reorganization and scattering. Next, we examined if expression of mutant-p53 can confer motility and promigratory properties to cells receiving TGFβ. To this end, we monitored the *in vitro* behavior of control and p53H175R expressing cells in a wound healing assay, in which cells are induced to distrupt cell-cell contact, polarize and migrate into a wound created by scratching confluent cultures with a pipette tip. After 24 hours of TGFβ treatment, while p53-null cells had migrated poorly, p53H175R expressing cells almost completely invaded the wound (Fig. 1D). To control that this effect was not due to a bias in proliferation, we monitored BrdU incorporation and

found no difference between control and mutant-p53 expressing cells, irrespective of TGFβ treatment (data not shown). As an independent mean of measuring cell motility, we examined the behavior in transwell-migration assays of parental, wild-type or mutant-p53 reconstituted H1299 cells. Figure 1E shows that expression of mutant-p53 parallels with the acquisition of a TGFβ pro-migratory response also through a reconstituted basement membrane.

This result clearly indicates for the first time that, at least in *in vitro* migration assays, a mutation in a Smad cofactor can turn upside-down the biological response to TGFβ, from a cytostatic response (in the case of wild-type p53) to a pro-migratory effect (coupled with mutant-p53).

Mutant-p53 is required for TGFβ -driven invasion and metastasis in breast cancer cells.

Our data link the gain of mutant-p53 to TGFβ-induced epithelial plasticity and migration, phenotypes whose emergence is critical for TGFβ invasive properties (Gupta and Massague, 2006). However, the actual requirement for these effects of mutant-p53, endogenously expressed in metastatic cancer cells, remained a key unanswered issue. To address this, we transiently knocked-down endogenous p53R280K expression in MDA-MB-231, a well-established cellular model system of invasive breast cancer. Parental MDA-MB-231 cells are quasi-mesenchymal, as they do not express E-cadherin and do express vimentin, and previous studies showed that their invasiveness *in vivo* and *in vitro* relies on autocrine TGFβ (Biswas et al., 2006). To study the endogenous role of mutant-p53, cells were transfected singularly with two independent siRNA targeting endogenous p53 mRNA (siRNA A and B) or with a control siRNA (Fig. 3C). As shown in Figure 2A TGFβ induced a potent promigratory response in control cells (transfected with an unspecific siRNA, lane 1) cells as assayed by transwell-migration assays. This effect appeared Smad-dependent, as it was abolished by Smad4 knock-down (lane 2). Remarkably, TGFβ-induced motility of mutant-p53 transiently depleted-MDA-MB-231 was also dramatically reduced (Fig. 2A, lane 3 and 4). The results of the two independent siRNA against mutant-p53 are very similar, thus indicating that the biological effect of mutant-p53 depletion is specific and not due to an off-target effect of the siRNA. We then addressed the requirement of mutant-p53 in a more complex experiment, namely Matrigel evasion assay, that recapitulates three aspects of the *in vivo* metastatic process: adhesion, extracellular matrix degradation and migration (Albini, 1998). In this set-up, cells are embedded in a drop of Matrigel matrix containing extracellular proteins (collagens, laminin) and growth factors. As shown in Figure 3A, parental MDA-MB231 can exit from the drop, this behavior is inhibited by treatment with the TGFβ receptor inhibitor SB or by depletion of mutant-p53. This was accompanied by changes in the morphology of the cells: within the Matrigel, control (shGFP) cells displayed a mesenchymal shape and protrusions, but these were lost after

inactivation of TGFβ or depletion of mutant-p53 (Fig. 3B). These data suggest that mutant-p53 and TGFβ jointly control cell shape, *in vitro* migration and invasiveness of breast cancer cells.

Multiple evidences indicate that the metastatic spread of MDA-MB-231 cells *in vivo* is under control of autocrine TGFβ (Arteaga et al., 1993; Bandyopadhyay et al., 1999; Deckers et al., 2006; Padua et al., 2008). To test if mutant-p53 is relevant for TGFβ-promoted malignant behaviors *in vivo*, cells were transduced with retroviral vectors expressing either an established shRNA sequence targeting p53 RNA (the same of siRNA B) or shGFP, and then drug-selected to enrich for positive transfectants (Fig. 3C). In this way the silencing siRNA was consitutively overexpressed under H1 promoter keeping the targeted mRNA to a low level. We injected control (shGFP) or stably mutant-p53 depleted (shp53) MDA-MB-231 cells into the mammary fat pad of immunocompromized mice. The two cell populations grew at similar rate *in vitro* and formed primary tumors at similar rates and size *in vivo* (data not shown and Fig. 2B), indicating that high levels of mutant-p53 in MDA-MB-231 cells are not essential for proliferation or for primary tumor formation. Six weeks after implantation of shp53 or shGFP knocked-down MDA-MB-231, mice were sacrificed and examined for presence of metastatic lesions. In agreement with previous reports, we found that orthotopically injected MDA-MB-231 are very poorly metastatic to the lung, but efficiently metastasize to the lymphnodes (Dadiani et al., 2006). To quantify metastatic spread, we monitored the weight and histological appearance of the controlateral lymph node, a well-established read-out of systemic disease in human breast cancers. Strikingly, depletion of mutant-p53 drastically reduced the number of lymph node metastases when compared to the control cells, as only one out of 22 mice injected with the shGFP cells scored negative for lymphonodal metastasis, whereas 10 out of 22 of mice carrying the shp53-depleted tumors remained metastasis-free (Figure 2C). To further validate the change in metastatic ability between MDA-MB-231 shGFP and shp53, we performed tail vein injection in nude mice. After four weeks, mice were sacrificed and analysed for pulmonary metastasis. In animals injected with control cells, lungs appear dramatically infiltrated (Fig. 2D and 2E) with severe disruption of the lung parenchima. Strikingkly, lungs from mice injected with depleted cells showed only microscopical metastasis (Fig. 2D and 2F). As specificity control, metastatic behavior of shp53-MDA-MB-231 cells is rescued, *in vitro* and *in vivo*, by adding back siRNA insensitive mutant-p53, but not wild-type p53 to a single clone of shp53-MDA-MB231 (Figure 2A, compare lanes 7, 8, 9; Figure 2D, compare lanes 4, 5 and 6. Fig.3C for expression control). These experiments have been carried out in collaboration with Dr.ssa Maddalena Adorno, Dr. Michelangelo Cordenonsi (from our group) and Dr. Antonio Rosato (IOV).

p63 is downstream of mutant-p53 and opposes TGFβ -induced malignant responses

Knock-in mice expressing mutant-p53 (p53+/R172H or p53+/R270H) develop metastatic carcinomas, a phenotype never observed in mice simply lacking one p53 allele (p53+/-) (Lang et al., 2004; Olive et al., 2004). Intriguingly, loss of one allele of p63 or p73 similarly endows p53 +/- tumors with metastatic properties (Flores et al., 2005). The parallel between loss of p63/p73 and gain of mutant-p53 is compatible with mutant-p53 acting as a restraining factor for the activity of its family members (Li and Prives, 2007). Interestingly, loss of p63 or p73 fosters progression, but in distinct tumor spectra, with loss of p63 specifically promoting the emergence of metastatic cancers in stratified epithelia (Flores et al., 2005), which tumor types are characterized by a clear promalignant-switch in TGFβ responses. Moreover it has been suggested that mutant-p53 may acquire additional functions through its interaction with the p53 family members p63 and p73 (Vousden and Prives, 2005).

These hints prompted us to test the role of p63 in cell migration and invasion induced by TGFβ. We first addressed the role of p63 in the cellular system analyzed so far, H1299 and MDA-MB231 cell lines. In the latter case we transiently overexpressed two isoforms of p63 (TA and ΔNp63α), this caused a marked inhibition of TGFβ-induced transwell migration (Figure 4A). Conversely, siRNA-mediated depletion of p63 in parental H1299 cells empowers TGFβ-induced migration, phenocopying gain of mutant-p53 (Figure 4B). We then tested the epistatic relationships between mutant-p53 and p63. If the loss of migration phenotype observed in sip53-MDA-MB231 was dependent on p63, than the double depletion of p63 and mutant-p53 should lead again to a migratory response after TGFβ stimulation. Consistently, loss of p63 leads to a remarkable rescue of TGFβ promigratory and proinvasive properties in p53-depleted MDA-MB-231 cells (Figure 4C, lanes 3 and 4). To confirm this result *in vivo* we stably antagonized p63 activity by overexpressing p63DD in shp53-MDA-MB231 with lentiviral deliver system. p63DD is a fusion protein consisting of EGFP fused in frame with p63 tetramerization domain, in this way it is able to oligomerize with the endogenous p63 and sequester it, acting as a dominan negative protein. The usage of this dominant negative form of p63 allowed us to inhibit p63 activity to a larger extent compared to the stable knock-down of p63 expression with an interfering short-hairpin RNA. The inhibition of p63 activity was controlled in H1299 cells, with a luciferase transcriptional assay for a reporter plasmid for p63 (Fig. 4F). Remarkably, p63 inactivation substantially rescues lung colonization in mutant-p53-depleted cells (Figure 4E). Taken together, the evidences *in vitro* and *in vivo* suggest that TGFβ uses mutant-p53 to surpass the barrier that p63 raises against TGFβ-induced malignant cell responses (Figure 4D).

A ternary complex between mutant-p53, p63 and Smad.

We next sought to address the mechanism by which TGFβ controls p63 through mutant-p53. Previous work has shown that, at the biochemical level, the recombinant core domain of some mutant-p53 proteins, but not of wild-type p53, binds and inhibits p63 by masking its DNA binding domain (Gaiddon et al., 2001; Strano et al., 2002). However, several observations suggest that this biochemical model is an oversimplification, that misses at least one essential component. Indeed, to be effective as an antagonist, mutant-p53 should be able to quantitatively titrate p63; in contrast, there is scant evidence that such interaction can effectively occur *in vivo* at physiological concentrations of these proteins (Caulin et al., 2007; Li and Prives, 2007 and see below). Moreover, stratified epithelia almost exclusively express ΔNp63α, an isoform *per se* unable to complex mutant-p53 (Gaiddon et al., 2001).

We tested if Smads and FGF/Ras pathway were the physiological driving forces that push mutant-p53 to bind p63, finally inhibiting it. For this purpose we perfomed co-immunoprecipitation assays in different cell lines, each appropriate to emphasize a different aspects of the model. We first immunoprecipitated endogenous mutant-p53 from Hacat keratinocytes (carrying the p53H179Y/R282W mutations), a cell line that expresses high level of ΔNp63α protein. Co-precipitating proteins were revealed by western blotting. In lysates of untreated cells we could detect only a weak interaction between p63 and mutant-p53, but this association was massively augmented in the presence of TGFβ signaling (by more that 20 folds; Figure 5A, compare lanes 2 and 3). Crucially, endogenous Smads are essential for mutant-p53/p63 complex formation, becoming this undetectable upon transfection of siRNA against Smad2/3 (Figure 5A, compare lane 3 and 4). These findings suggest that TGFβ signaling is an essential determinant for mutant-p53 to complex its family member p63. In an alternative experimental set-up, coimmunoprecipitation using anti-Smad2 antibodies reveals Smad2 associated with p63 and mutant-p53 (Figure 5B); yet, while the interaction of Smad2 with p63 is to a large extent independent from mutant-p53 (Figure 5B, lane 3), Smad binding to mutant-p53 requires p63 (Figure 5B, lane 4), suggesting that mutant-p53 preferentially associates to a preassembled p63/Smad2 scaffold in these cells. Together, these biochemical data indicate the formation of a TGFβ-induced ternary complex between endogenous p63, mutant-p53 and Smads.

We then studied if this biochemical model could be confiermed in MDA-MB231 cells. For this, we immunoprecipitated endogenous mutant-p53 from MDA-MB-231 cells, that express low levels of p63, and revealed co-precipitating proteins by western blotting (Fig. 5C). Using lysates of untreated cells we could not detect any interaction between p63 and mutant-p53, but this association

appears only in the presence of TGFβ signaling (Fig. 5C, compare lane 1 and lane 2). Crucially, endogenous Smads are essential for mutant-p53/p63 complex formation, as this becomes undetectable upon transfection of siRNA against R-Smads (Fig. 5C, compare lane 2 and 3). These findings suggest that TGFβ signaling, either exogenously provided or endogenously present, is an essential determinant for mutant-p53 to complex its family member p63. These experiments have been carried out in collaboration with Dr. Michelangelo Cordenonsi.

Ras regulates mutant-p53/p63 association.

Next, we investigated the determinants that regulate the association of mutant-p53 and Smads. A wealth of evidence in cancer cells and animal models clearly indicates that metastasis require the combination of TGFβ signaling and elevated Ras signaling, at least in several epithelia, but the mechanisms of this intersection remain unclear (Cui et al., 1996; Grunert et al., 2003; Muraoka et al., 2003; Oft et al., 2002; Siegel and Massague, 2003). Interestingly, the same signaling pathways are involved in mesoderm development in *Xenopus* embryogenesis, where, remarkably, it is wild-type p53 that serves as an essential link, being the formation of the p53/Smads complex dependent on FGF/Ras/Raf/MAPK/CK1δ/ε-mediated phosphorylation the p53 N-terminus (Cordenonsi et al., 2007). This precedent prompted us to test if Ras signaling may be also essential for Smad recognition by mutant-p53. To assay this hypothesis, we treated cells with a MEK-inhibitor drug (PD325901) and observed that endogenous oncogenic Ras is indeed required for mutant-p53 N-terminal phosphorylation (Figure 5F) and for the formation of the TGFβ-induced ternary complex (Fig 5C). Consistently, as shown in Figure 5F and 5H respectively, depletion of CK1δ/ε or mutation of the Ras/CK1δ/ε-targeted phosphorylation sites of mutant-p53 abolished ternary complex formation in MDA-MB231 and reconstituted H1299 cells (expressing oncogenic N-Ras).

Besides the biochemical evidencies that clearly show the requirement of mutant-p53 N-terminal phoshorylation by FGF/Ras/CK1δ/ε pathway for the formation of the ternary complex at a physiological level, we wanted to address if those inputs match the requirements for the TGFβ-driven migration phenotype. The biological results in transwell assays strikingly parallel the biochemical changes, as treating either MDA-MB231 or H1299-p53H175 cells with MEK small inhibitory compound PD325901 diminishes the TGFβ-driven migration, and the same result can be obstained with the depletion of CK1δ/ε, the kinase downstream of FGF responsible for p53 N-terminal phosphorylation (Fig. 5D). We finally validated *in vivo* the role of CK1δ/ε and found that CK1δ/ε-depleted MDA-MB-231 failed to undergo metastatic spread after tail vein injection in recipient mice (Figure 5E). Together, data presented so far indicate that Ras/CK1δ/ε signaling enables ternary complex formation and empowers TGFβ-induced migration and breast cancer cell

metastasis. These experiments have been carried out in collaboration with Dr. Michelangelo Cordenonsi.

A Smad bridge allows mutant-p53 to inhibit p63.

The evidences shown in Figures 5A and 5C, demonstrate that mutant-p53 requires Smad to contact and inhibit p63, this moved our attention to the study of the domains required for the ternary complex formation. It has already been shown that p53 binds to the N-terminal domain of Smad2/3 (MH1 domain), leaving the C-terminal domain (named MH2) free to interact with other proteins, for example FAST-1 and Smad4 (Dupont et al., 2004). In our previuos work we proposed that, to be effective at a physiological level, the interaction between p53's TA domain and MH1 needs the contribution of Ser6 and Ser9 phosphorylation by FGF/Ras/CK1δ/ε pathway. p63 shares some structural similarities with its homologue p53, but shows also important differencies, for example the longer isoforms of p63 have three structural C-terminal domains that have no counterpart in p53, namely SAM (Sterile α-Motif), QP (Proline-rich domain, called also TAD2, Transactivation Activator Domain 2), TID (Transactivation Inhibitory Domain). On the N-terminal side of both p53 and p63 resides the Transactivation Domain (TA), while its biological role is conserved (activation of transcription), the sequence homology is low, about 22% identity (Barbieri and Pietenpol, 2006). But unlike p53, p63 can also be transcribed from an alternative promoter that gives rise to ΔN isoforms, which lack the N-terminal TA domain and can still activate a specific set of genes (Murray-Zmijewski et al., 2006). The highest degree of homology is seen within the central DBD, which can explain why p63 can bind p53RE in the promoters of p53 target genes and activate their transcription.

We than thought to compare the different isoforms of p63 in their ability to bind *in vitro* a Glutathione-Sepharose matrix loaded with Smad3 or with the single MH1 or MH2 domains. The alternative splicing of p63 gene gave us a set of "natural deletion mutants" to analyze. Besides the existence of β isoform, with intermediate features, the main C-terminal isoforms of p63 are α (comprising SAM, QP and TID domain) and γ, that is interrupted after the oligomerization domain (Fig. 6A). Thus we *in vitro* synthetized TAp63α, TAp63γ, ΔNp63α, ΔNp63γ and tested the binding with the different peptides immobilized on the resin. We discovered two isoforms of p63 that clearly interacts with different Smads' domains: while ΔNp63α strongly binds MH2 domain, TAp63γ stably interacts with MH1 (Fig. 6A). Given the structural differences between the two structures it is easy to map the interactions in the α domain, for ΔNp63α, and in the TA domain, for TAp63γ isoform. One would expect that, if these were the two interaction surfaces, the TAp63α isoform should contact both the MH1 and MH2 domains with the same intensity, this is what we observed in this set up, but the interactions were weaker compared to those of ΔNp63α and TAp63γ

isoforms (Fig. 6A). However it is already reported that the C-terminal domain of p63, and specifically the TID domain, can fold back and inhibit TA domain (Serber et al., 2002), probably masking the interaction surface with Smad3 MH1. While mapping Smad interaction in the TA domain confirms previous findings with p53 (Cordenonsi et al., 2007), the identification of a second Smad interaction surface in the α domain of p63 is interesting because the vast majority of p63 is expressed *in vivo* as ΔNp63α isoform, lacking TA-domain (Yang et al., 1998). We then wanted to further dissect the domain responsible for the interaction between the C-terminal region of p63 and Smad3 MH2 domain. To this end we expressed each single C-terminal domain, SAM, QP and TID and assayed for the *in vitro* binding to immobilized GST-MH1 and GST-MH2. Coherently with the previuos findings, the only detectable interaction was between MH2 of Smad3 and the TID domain of p63 (Fig. 6A). These structural hints suggest that RSmad, by means of its N- and C-terminal domains may serve as a platform to assemble the mutant-p53/p63 complex (Figure 6B).

To test the hypothesis that this configuration might inhibit p63 transcriptional properties we first monitored p63 transcriptional activity in luciferase assay. We took advantage again of H1299 cellular model system where we have been able to screen the effects of different mutant-p53 isoforms, corresponding to hot-spot mutation in human cancers, in a context of TGFβ stimulation. As shown in Fig. 7A the reporter plasmid was highly activated by overexpression of p63 and neither co-transfection with wild-type p53 nor TGFβ treatment significantly modified p63 activity (Fig. 7A and 7B). Conversely, if some mutant-p53 were singularly cotranfected with p63, we observed a clear inhibition of p63 induced transcription of the reporter plasmid (Fig. 7B). Notably the inhibition is effective only in the presence of TGFβ stimulation, while the mutant-p53 isoforms alone were uneffective on p63 activity.

Mechanism of p63 inhibition.

We could envision at least three hypotheses regarding the mechanism of p63 inhibition by the ternary complex. The first one is that, once trapped within the complex, p63 could no more bind its recognition sites. The second idea is that p63 could still bind its promoter elements but it is unable to recruit transcriptional activators and PolII machinery; the third hypothesis, p63 binds the promoters, but the complex with mutant-p53 and Smad contacts transcriptional repressors instead of activators.

To discriminate between these hypotheses we carried out ChIP analysis for p63 in the same set up used for the luciferase studies. We used a mix of estabilished polyclonal antibodies for p63 to ensure an efficient immunoprecipitation of the DNA bound complex, taking as p63BE the p53 recognition site present and activated in the reporter plasmid. In this way we could look to p63 behaviour in *in vivo* interaction with a binding element while adding each single component of the

ternary complex. As expected, we were able to amplify efficiently the p53BE plasmid region after pull-down of p63, meaning that p63 is interacting with that region *in vivo* (Fig. 7C). In line with the luciferase and biochemical data, overexpression of mutant-p53 alone is unable to modify the affinity of p63 for its binding element (Fig. 7C, Lane 3). However, after TGFβ treatment, and thus activated Smad bridging, mutant-p53 is able to cover the DNA interaction surface of p63 (Fig. 7C, Lane 4). We then moved to estabilished endogenous p63 binding elements of the CDK1A gene (Deyoung and Ellisen, 2007) with the same results. Thus, incorporation of p63 into a TGFβ-induced ternary complex impairs p63 binding to DNA *in vivo*.

p63 titration by mutant-p53 and Smad regulates metastasis.

During malignant progression, sequential elevations of TGFβ/Smad signaling is associated with the acquisition of metastatic potential (Cui et al., 1996; Oft et al., 2002). We thus explored the possibility that the metastatic shift of cancer cells could correspond to a quantitative inactivation of p63. For this, we monitored the dynamic of the trimeric complex in locally invasive D3 spindle carcinoma cells and their metastatic derivative D3S2, bearing constitutive Smad activity but expressing equal levels of p63, mutant-p53 (p53C236F) and oncogenic Ras (Oft et al., 2002: Figure 8A). Cell lysates were immunoprecipitated with anti-p53 antibodies and co-precipitating p63 quantified by western blotting. The amount of p63 complexed by mutant-p53 raised dramatically upon TGFβ treatment in D3 cells (becoming 50% of the input), to become essentially quantitative (>95%) in metastatic D3S2 cells (Figures 8B and 8C). Thus, in advanced tumors, increasing doses of TGFβ/Smad2 signaling correspond to increasing levels of p63 trapped into mutant-p53-containing complexes.

D3S2 cells allow to validate *in vivo* the requirement of mutant-p53 and oncogenic Ras/CK1δ/ε signaling in a cellular context rendered metastatic by elevated Smad signaling (Figure 8F). As shown in Figure 8D, mutant-p53, high levels of oncogenic Ras and CK1δ/ε activity are required for lung metastasis of D3S2 cells upon tail vein injection in immunocompromised mice. This closely recapitulates our previous findings in human breast cancer cells, suggesting a general impact for the mechanism here described in TGFβ-driven malignancy. Further challenging the mutant-p53/p63 axis, we also tested in D3S2 whether tipping back the balance by raising p63 levels was sufficient to confer metastasis protection. For this, we stably transduced D3S2 with ΔNp63α expression construct (D3S2-p63), and monitored lung colonization upon intravenous injection in recipient mice. D3S2-p63 cells displayed a remarkable 80% reduction of metastatic nodules when compared to parental D3S2 (Figures 8G). Notably, p63 expression did not impair tumor growth *per se* (data not shown). Thus, rebalancing the mutant-p53/p63 ratio specifically inhibits metastatic proclivity, underlining how even advanced cancer cells retain exquisite sensitivity to p63 activity.

These experiments have been carried out in collaboration with Dr.ssa Maddalena Adorno, Dr. Michelangelo Cordenonsi and Dr. Antonio Rosato (IOV).

A TGFβ invasive program.

To identify the TGFβ invasive and metastatic program in breast cancer cells, we carried out Affymetrix microarray studies on control and TGFβ treated MDA-MB-231 cells. We found that TGFβ regulate 448 genes (Fig. 9A, see Methods for detail): TGFβ coordinates a complex interaction between the cytoskeleton and the extracellular environment. Among the gene list, several genes had been previously described as direct Smad targets, such as PAI1/SERPINE1, JunB and Smad7. The successful identification of these genes validated our approach to identify novel genes that may play equally important roles in TGFβ induced metastasis. Of all the targets, biological function was previously reported for about 300 genes. Remarkably, many of these (155) have been previously implicated in cell movement, invasion or metastasis, either in breast of other contexts. What follows is a description of these targets and their tentative classification in functional categories.

TGFβ induces both extracellular matrix components that favors cellular movements (COL1A1, COL5A1, COL27A1, LAMC2, Fibronectin/FN1, Thrombospondin-1/THBS1) and enzymes involved in the ECM remodelling (ADAMTS6, ADAM19, (PAI-1/SERPINE1, u-PA/PLAU). TGFβ also promotes the integrin-based ECM-cell adhesion by inducing an integrin (ITGAV), integrin modulators (PLEKHC1, TSPAN2) and by the formation of focal adhesion structures through induction of a Rho small GTPase (RHOB) and various Rho activators (NEDD9, M-RIP, RAPGEF2) and the repression of some Rho inhibitors (ARHGAP25, ARHGEF2, ARHGAP24 and ARHGAP12). Rho, in turns, is well known to promote the formation of actin stress fibers, whose contraction in instrumental for cellular movement. This contraction may be further enhanced by TGFβ through induction of some motor proteins (TAGLN, TPM1) and the activation of the inositol/Calcium pathway through secretion of Endothelin-1 (E_N1). TGFβ induces components of cAMP (PKIA, HTR1D), semaphorine (PLXNA2, NRP2, RND1) and ephrine (EPHA4, EPHB2) signaling pathways that allow the cell to locally inhibit Rho activity in response to extracellular signals. Conversely TGFβ also induces the Wnt ligand WNT5A, that activates Rho through the Planar cell polarity pathway. This suggests that the local activation of these pathways would allow the polarization of the cellular movements, probably resulting in the repulsion of the cells one from the other. TGFβ also promotes formation of filopodia at expenses of focal adhesion, by inducing several genes involved in this process (Moesin/MSN, FGD4, MYO10 and RHOF). Rac-induced lamellipodia formation can be indirectly promoted by TGFβ through the

induction of various ligands for Receptor Tyrosine Kinases (PDGFA, PDGFB, NGFB, FGF5, HBEGF) that activate the PI3K pathway. Phospho-inositol will eventually promote cellular movement by activating two other TGFβ-induced protein: the pro-metastatic kinase NUAK1 and the Rac activator TIAM2. This activation would probably occur in the proximity of cell-ECM junctions as TGFβ, by inducing the scaffold protein LIMS1, favors the activation of RTKs in the context of focal adhesive structures. The RTK pathway is further promoted by TGFβ through the repression of RAS inhibitors (SPRED1, SPRED2, SPRY1), the induction of the RAS activator RASGRP1 and of some RAS downstream effectors (JUNB, JUN, ETS1, ETS2). TGFβ also modulates other genes important for metastasis but that cannot be immediately connected to the program so far presented: cadherin family members (CDH19, PCDH1, PCDH20, PCDH18, FAT3), the Notch ligand Jagged1 (JAG1), some repressors of the hedgehog pathway (KCTD11, HHIP), Interleukin 1 (IL11), ligands and receptors for the TNF pathway (TNFRSF12A, TNFSF10, FAS, TNFSF4, TNFSF18) and modulators of the microtubular cytoskeleton (TUBA1, CXADR, TBC1D8).

A mutant-p53/Smad invasive signature.

Loss-of-mutant-p53 does not affect expression of canonical markers of TGFβ-mediated EMT (data not shown); moreover, alteration of mutant-p53 expression is effective for metastasis in cells that are already mesenchymal (such as MDA-MB231). This suggests that the ability of mutant-p53 to drive TGFβ-induced cell migration and invasion relied on the regulation of a very specific gene network. More specifically, we were interested in identifying the genes that are regulated by p63 and that mediate anti-metastatic activity.

To recognize the p63 targets involved in opposing TGFβ induced malignancy (rather than mutant-p53-only or general targets of p63) we focus on the much more restricted number of TGFβ targets whose up- or downregulation required mutant-p53. To do this, we compared the transcriptomic profile of shGFP and shp53 MDA-MB-231 cells either untreated or treated with TGFβ by using Affimetrix microarrays. Indeed, out of the hundres of TGFβ regulated genes only a small minority (n=17) was opposed by mutant-p53 depletion. In light of the biological requirement of mutant-p53 for metastasis, these molecular data are consistent with the following model: first, that the TGFβ prometastatic program identified above is insufficient, per se, to drive malignant cell behavior until p63 is active; second, that the mutant-p53/p63 axis must operate through a restricted set of metastasis-controlling genes.

As shown in Fig 9E, after validation by Northern Blot, we were able to confirm the expression of just five genes: two are upregulated (*GPR87* and Follistatin/*FST*) and three are downregulated by TGFβ (*ADAMTS9*, Sharp1/*BHLHB3* and Cyclin G2/*CCNG2*) only in the

presence of mutant-p53. As for the TGFβ induced genes, G-protein-coupled receptor 87 (*GPR87*) is an orphan G-protein coupled receptor and Follistatin is a well-known extracellular inhibitor of the TGFβ pathway, specifically for Activin and BMP ligands. We decided to not further characterize those genes as *GPR87* is poorly induced by TGFβ in MDA-MB-231, and *FST* could be redundant with Follistatin-like 3 (*FSTL3*), whose expression is mutant-p53 independent. In particular, we focused on two, so far poorly characterized genes, *Sharp-1* and *Cyclin G2*, that are negatively regulated by TGFβ via mutant-p53: this suggested a role as metastasis suppressors. To verify these molecules as positive targets of p63, control and p63 siRNA-depleted MDA-MB-231 cells were assayed for gene expression by quantitative RT-PCR. Loss of p63 potently inhibited the expression of *Sharp-1* and *Cyclin G2*, an effect phenocopied by TGFβ treatment in control cells (Figure 9C). Of note, TGFβ had no effect in p63 knock-down cells, suggesting that TGFβ has no additional, p63-independent, repressing effects.

To functionally validate these genes as effectors of the mutant-p53/Smad/p63 pathway, we carried out epistasis experiments testing if depletion of Sharp-1 or Cyclin G2 could rescue TGFβ induced migration in p53-depleted cells. As shown in Figure 9D, siRNA-mediated knockdowns of Sharp-1 or Cyclin G2 restore TGFβ dependent pro-migratory activities in shp53 MDA-MB-231, phenocopying p63-depletion. Thus, these molecules mediate the antagonizing effect of p63 on TGFβ proinvasive responses.

Finally we tried to unify our biochemical mechanism with the target genes came out from the microarray analysis. The transcription regulation of our candidate genes is even less characterized than the function of the genes itself. Other groups tried to identify the p63 binding element in the whole genome through a ChIP on CHIP assays, the main problem connected to this kind of approach is that only the most strongly regulated regions are detected, while the majority of the binding elements, being cell-type specific, are often lost. Moreover, the genome wide analysis for p63 where all carried out in keratinocytes, cells bearing ΔNp63α, while MDA-MB231 cells shows only TAp63α expression. For these reasons we analyzed from scratch the genomic locus of one of our two target genes, Cyclin G2, trying to recognize p63-binding motifs. To this purpose we took advantage of a published algorithm (p53MH, Hoh et al., 2002) that scans an input sequence for p53 consensous sites. We submitted to the algorithm 30Kb of the genomic locus containing Cyclin G2 gene and obtained 15 candidate sequences that we validated with ChIP analysis (data not shown). To avoid false positive results we compared the ChIP analysis from control MDA-MB231 and from cells depleted of endogenous p63 and found that a site within the second intron was specifically bound by p63 (Fig. 10A, lower panel). Once having known which is the *in vivo* binding element of p63 in Cyclin G2 locus, we assayed the behaviour of this binding in response to TGFβ.

We then repeated the ChIP experiment in shGFP and shp53 MDA-MB231 either treated or untreated with TGFβ. Strikingly, TGFβ was able to take off p63 from its binding site only in the presence of mutant-p53 (Fig. 10A, upper panel). This genomic regulation data perfectly pairs with the biochemical and biological findings and support the model in which activated Smad allows the quantitative relieve of p63 by mutant-p53 from the binding site of metastasis suppressor genes.

Clinical validation of Sharp-1 and Cyclin G2 (collaboration with Prof. Silvio Bicciato and Dr. Aldo Solari, University of Padua, University of Modena e Reggio Emilia).

Current treatment indication and prognosis largely derive from histopathological analyses of the primary tumors, on involvement of axillary lymph nodes and expression of ER receptors. While useful, these parameters are weakly correlated with the genetic status of a tumor and are poor predictors of its oucome: indeed, two patients with the same stage of breast cancer can display very different risks of recurrence and metastasis. Tackling this problem, researchers are associating expression of specific gene sets, or "signatures", to particular aspects of tumor biology and classification. These signatures have been shown effective in predicting disease-free survival, or risk of developing metastasis in primary tumors. The ultimate goal of these studies is to aid clinicians in tailoring the most appropriate treatements.

Here investigated the clinical relevance of Sharp-1 and Cyclin G2 expression in human tumors. If the detection of Sharp-1 and Cyclin G2 in human primary tumors is biologically meaningful, one might expect that reduced expression of these genes should be associated with poor clinical outcome. Of note, Sharp-1 and Cyclin G2 are not contained in known signatures for breast cancer metastasis, i.e. the "70-genes signature", the "recurrence score" or others (Fan et al., 2006). To evaluate the prognostic value of Sharp-1 and Cyclin G2 (henceforth "minimal signature"), we took advantage of the available gene expression datasets summing up to 1200 primary breast cancers with associated clinical data, including survival and distant recurrence (Table 1). In this way we could give to our study more reliability and evaluate the robustness of the minimal signature when applied to different cancer subtypes, histology and origins. We defined in each dataset two groups of tumors with respectively high and low level of expression of Sharp-1 and Cyclin G2 (Figures 11A-E) (see Experimental Procedures for statistical analyses) and used Kaplan-Meier analysis that permits to estimate the survival function from life-time data, dinamically taking in account losses of patients before the final outcome is observed. By default, in Kaplan-Meier plots the vertical axis represents estimated probability of survival for a hypothetical cohort during the period indicated in the x-axis, while the p-value of the log-rank test reflects a significant association between *minimal signature High* and longer survival. Strikingly, when tested using the univariate Kaplan-Meier survival analysis, the group expressing low levels of the minimal signature ("Low")

displayed a significant higher probability to develop recurrence when compared to the "High" group in all the dataset analyzed (p-values ranged from 0.02 to 3E-05, depending on the datasets) (Figures 11A-E). Interestingly, the minimal signature performed comparably to the 70-genes profile in stratifying patients according to their clinical outcome (Figures 11A-E, compare left plot with right plot) and is associated to risk of distant metastasis to both bone and lung (Figure 12A). This was a great result because the 70-genes profile is considered one of the best gene suite tool and was already approved by FDA in 2007 to calculate the prognosis for development of distant metastasis in patients with negative lymph nodes.

To further evaluate the prognostic value of the minimal signature we performed multivariate Cox proportional-hazards analysis on the 187 tumors dataset from National Cancer Institute and 295 tumors from the NKI database (Fan et al., 2006; Sotiriou et al., 2006). Whereas the Kaplan-Meier method with log-rank test is useful for comparing survival curves in two or more groups, Cox proportional-hazards regression allows analyzing the effect of several risk factors on survival. With this method, we could evaluate the minimal signature in the context of some variables commonly used in the clinical practice, such as estrogen-receptor status, tumor diameter, nodal status, tumor grade and treatment status. As shown in Table 2, Figure 13 and 14, the minimal signature remained a significant predictor of metastasis-free survival. Furthermore, the minimal signature is an independent predictor of survival that adds new prognostic information to established clinical predictors such as size, node status, tumor grade, ER status, age and treatment (Table 2, Figure 13 and 14). This means that if we stratify patients into two groups according to known clinical predictors, for example those with large or small tumors (Fig. 13A, upper panels), and than we analyze the two populations with the minimal signature, we are able to identify two further subgroups for each population. In the case of tumor size plus minimal signature stratification (Fig. 13A, upper right panels), within the patients with tumors larger than 2 cm we can recognize two further subgroups, and those who express high level of Sharp-1 and Cyclin G2 have a prognosis similar to patients with small tumors (lower than 2 cm). Moreover, we tried to apply the minimal signature to breast tumors histologically classified as grade 2 according to the Nottingham grading scale (Elston and Ellis, 1991), that is a subtype of mammary cancer that presents an intermediate prognosis and whose therapeutic management is difficult to asses. The rational of this analysis was to probe if our signature could be informative for the clinical treatment, as grade 2 tumors are intermediate between grade 1 (well differentiated/slow growing and with good prognosis) and grade 3 (poorly differentiated, invasive and displaying bad prognosis). Intriguingly, when applied to grade 2 tumors of multiple independent datasets, the minimal signature resolved these patients into two groups with outcomes comparable to grade 1 (good prognosis), and therefore unlikely to receive

benefit from adjuvant therapy, and grade 3 (bad prognosis), that should be therefore aggressively treated (Figure 15).

In sum, the clinical validation as prognostic tool of Cyclin G2 and Sharp-1, two targets of the TGFβ/mutant-p53/p63 axis, supports the general relevance of the mechanisms here described for breast cancer metastasis.

DISCUSSION

The biology of mutant-p53 has been the focus of intense investigation. This protein is unable to bind its cognate DNA binding sites, suggesting that its expression is selected in cancer cells to provide some form of neomorphic oncogenic function, generally defined as the "mutant-p53 gain-of-function" phenomena (Soussi and Lozano, 2005). A major advancement in the understanding of mutant-p53 biology has been the generation of transgenic mice expressing p53R172H and p53R270H using the knock-in technology (Lang et al., 2004). Comparison of these mice with those inheriting a p53-null allele revealed that mutant-p53 expression fosters metastasis, a phenotype rarely found in mice with a p53-null allele.

The ability of p53 to switch from friend to foe depending on its mutational status presented striking analogies with the switch in TGFβ responsiveness reported in many cancers: TGFβ is a tumor suppressors of early neoplasms but, at later stages of the diseases, it becomes a potent prometastatic factor, fostering cancer cell migration, epithelial-mesenchymal transition and stromal invasion (Derynck et al., 2001).

Prompted by the cooperation between wild-type p53 and Smad, we therefore investigated the role of mutant-p53 in TGFβ responsiveness. Here, we describe a new signaling pathway that instills metastatic proclivity to epithelial cancer cells:

TGFβ -->Smad/mutant-p53 --| p63 --> metastasis protection.

This model incorporates several elements of novelty and discussion:

We propose that gain-of-TGFβ metastatic properties can be acquired by the combined action of two common oncogenic lesions, Ras and p53-mutation. Gain of mutant-p53 expression in noninvasive tumor cells empowers TGFβ pro-invasive and migratory abilities, whereas loss of mutant-p53 expression in aggressive tumors impairs their metastagenicity. A wealth of published data documented the requirement of Ras for TGFβ malignant responses but the mechanism of such interplay has not been addressed (Grunert et al., 2003). Our data provide a step forward in this direction: Ras signaling promotes mutant-p53 phosphorylation and, in so doing, it is required for the formation of the mutant-p53/Smad complex. The critical role of mutant-p53 in metastasis has been recently suggested from elegant studies in transgenic mice, and this is particularly striking when expression of mutant-p53 is combined with oncogenic Ras (Caulin et al., 2007; Hingorani et al., 2005). In humans, p53 mutations are associated to poor prognosis in several types of tumors; intriguingly, p53-mutation is selected at very high frequency in aggressive HER-2 positive and basal-like breast cancers, that are particularly prone to metastasize (Sorlie et al., 2001). How and when a tumor acquires metastatic properties is unknown (Bernards and Weinberg, 2002). To our knowledge, the results here presented constitute the first indication that a particular combination of

two common oncogenic lesions, mutant-p53 and oncogenic Ras, selected to promote growth and survival of early neoplasms, also prefigure a cellular set-up with particular metastasis proclivity. This "passenger" trait will be exploited later on, during progression, to drive the metastatic switch, once cells gain access to high levels of TGFβ, either autonomously produced or extracted from the microenvironment.

The main mechanisms proposed for gain of function of mutant-p53 comprise the binding, the sequestration, and the inactivation of tumor suppressor proteins (Gaiddon et al., 2001; Strano et al., 2002). Among the possible mutant-p53 partners, the most intriguing is p63, as recent evidences using mouse models suggest that its interactions with mutant-p53 is important for its gain-of-function properties (Flores et al., 2005; Vousden and Prives, 2005). At the biochemical level, the recombinant core domain of mutant-p53, but not of wild-type p53, binds and inhibits p63 by masking its DNA binding domains (Strano et al., 2000). However, several observations suggest that this model may be an oversimplification. Firstly, in order to be effective as p63 antagonist, mutant-p53 should be able to quantitatively titrate its family members; in contrast, there is scant evidence that such interaction can effectively occur *in vivo* at physiological concentrations of these proteins. Secondly, only a subset of experimentally overexpressed mutant-p53 alleles can interact with p63 (Gaiddon et al., 2001). Finally, seminal work in compound p53, p63 and p73 heterozygous mice demonstrated that loss of p63 or p73 mimics the metastatic phenotype of mice carrying p53 point-mutations (Lang et al., 2004). Although this is in line with the view that mutant-p53 must somehow inhibits p63 activities, these biological data cannot be immediately explained by the simple physical interaction of p63 and mutant-p53, since the exceedingly abundant isoform p63 in tissues is ΔNp63α, that is unable to complex mutant-p53 (Gaiddon et al., 2001).

Here, we demonstrate that TGFβ/Smads signaling is the missing link between mutant-p53 and p63 inactivation and we estabilished a primary role for p63 as antagonist of TGFβ driven tumor invasiveness and metastasis. Mutant-p53 and Smad intercept p63 to form a ternary complex, in which the p63 transcriptional functions are antagonized. Thus, in presence of mutant-p53, TGFβ attains control over p63 and this unleashes TGFβ malignant effects. Indeed, mutant-p53 knock-down in metastatic cancer cells does not affect the expression of the TGFβ invasive program but rather forestalls its phenotypic exploitation. As expected from p63 being downstream of mutant-p53, inactivation of p63 transforms non-invasive cells into malignant tumors and rescues metastasis ability in mutant-p53-depleted breast cancer cells. Moreover, the quantal increase of Smad signaling that renders metastatic D3 carcinoma cells coincides with a quantitative loss of "free", uncomplexed p63. Strikingly, tipping back the balance by adding extra-p63 in these cells is sufficient to prevent such TGFβ -induced metastatic spread.

We previously showed that p53 family members and Smads cooperate for mesoderm development in Xenopus embryos and for growth arrest in mammalian cells, acting through independent binding elements in jointly-regulated promoters (Cordenonsi et al., 2003; Cordenonsi et al., 2007). Here we show that in metastatic cells p63 and TGFβ also play antagonistic functions. Indeed, in this context, Smads are not operating as transcription factors, but as adapters, bridging together mutant-p53 and p63. What may then determine the predominance of tumor suppressive vs pro-malignant responses to TGFβ? We propose that a crucial determinant is the relative distribution of p63 into three pools: free, bound to Smad2 in transcriptionally cooperating complexes, or instead inactivated into mutant-p53/Smad2 ternary complexes. Mutation of p53, the levels of Ras and p63, as well as the strength of TGFβ signaling, are critical variables in p63 distribution. During tumor progression, sequential elevations of constitutive Ras and Smad2 activity would foster a more and more quantitative incorporation of p63 into ternary complexes. Beside dampening the growth arrest response, this would progressively titrate away the anti-metastatic properties of free-p63. Finally, in advanced stages of the disease, quantitative inactivation of p63 would finally unleash TGFβ-driven metastasis.

We identified two genes, Sharp1 and Cyclin G2, differentially regulated by mutant-p53 that are the final downstream targets of the TGFβ/mutant-p53/p63 pathway. These were functionally validated *in vitro* as essential mediators of p63-mediated antagonism toward TGFβ responses. Traditional prognostic markers are able to confidentially assign prognosis to less than 50% of breast cancer patients. For the rest of the patients, new prognostic tools are required to assess the risk of metastasis and thus identify those that would benefit from adjuvant treatments (van 't Veer et al., 2002). Strikingly, in cancer patients, expression of Sharp-1 and Cyclin G2 represents a “minimal signature” with prognostic value independent from currently used clinical and histopathological variables. In spite of its simplicity, the minimal signature has predictive power comparable to more complex gene sets of predictors (Figure 8). The mechanism by which Sharp-1 and Cyclin G2 may act as metastasis suppressors *in vivo* remain ground for future studies. In the meantime, their use as diagnostic tools should be implemented for patients’ stratification in the clinical laboratory.

EXPERIMENTAL PROCEDURES

Migration and invasion assays

For wound-closure experiments, H1299 cells were plated in 6-well plates and cultured to confluence. Cells were scraped with a p200 tip (time 0), transferred to low serum and treated as described. Number of migrating cells were counted from pictures (five fields) taken at the indicated time points. Transwell assay were performed in 24 well PET inserts (Falcon 8.0 um pore size) for migration assays and in Matrigel-GFR coated PET inserts (Falcon) for invasion assays. For MDAMB-231, cells were plated in 10 cm dishes, transfected with siRNA or DNA plasmids and, after 8 hours, serum starved overnight. Then, 50000 or 100000 cells were plated in transwell inserts (at least 3 replicas for each sample) and either left untreated, treated with SB431542 (5 μM) or TGFβ1 (5 ng/ml). For H1299, cells were plated in the transwell in 10% serum but then changed to 0.2% serum. Cells in the upper part of the transwells were removed with a cotton swab; migrated cells were fixed in PFA 4% and stained with Crystal Violet 0.5%. Filters were photographed and the total number of cells counted. Every experiment was repeated at least 3 times independently. For matrigel invasion assay shown in Figure 3G, MDA-MB-231 and derivative cell lines were resuspended in drops (100 μl) of Matrigel Growth Factor Reduced (BD Biosciences), diluted 1:2 in DMEM/F12.

In vivo metastasis assays

Mice were housed in Specific Pathogen Free (SPF) animal facilities and treated in conformity with approved institutional guidelines (U.Padua and UCSF). For xenograft studies of breast cancer metastasis, shGFP- or shp53-MDA-MB-231 cells (1×10^6 cells/mouse) were unilaterally injected into the mammary fat pad of SCID female mice, age-matched between 5 and 7 weeks. After six weeks, mice were sacrificed and examined for metastases to lymph nodes. Macroscopic metastases to other organs were infrequent (liver, lung, peritoneum). Tumor growth in the injected site was monitored by repeated caliper measurements. For lung colonization assays, cells were resuspended in 100 μl of PBS and inoculated in the tail vein of SCID mice. Four weeks later, animals were sacrificed and lungs removed for the subsequent histological analysis. D3S2 and D3S2-p63 were also inoculated subcutaneously to evaluate the growth rate. The procedure for subcutaneous injection of mouse B9 squamous cancer cells was as previously described (Oft et al., 2002).

Protein interaction studies

To detect endogenous p63/Smad2/mutant-p53 complexes, cells were lysed by sonication in 20 mM Hepes, pH 7.8, 400 mM KCl, 5% Glycerol, 5 mM EDTA, 0.4% Np40, phosphatase and protease inhibitors, and cleared by centrifugation. For immunoprecipitations, extracts were diluted to 20 mM Hepes pH 7.8, 50 mM KCl, 5% Glycerol, 2.5 mM MgCl2, 0.05% NP40 and incubated with the appropriate proteinA-sepharose bound antibodies for four hours at 4°C. Prior to IP, beads were incubated overnight in PBS with 2% BSA and 0.05% CHAPS. After three washes in binding buffer, copurified proteins were analyzed by immunoblotting by using as secondary antibodies the ExactaCruz reagents (Santa Cruz biotechnology) to reduce the background from IgG. The amount of co-precipitated p63 was determined by quantification of western blots using ImageJ (NIH). PAB421 monoclonal antibody (Calbiochem) was used for p53 immunoprecipitations. For Smad2 IPs, we used the anti-Smad2 polyclonal antibodies (S-20, Santa Cruz biotechnology). The procedure for GST-pull down assays was described in Cordenonsi et al., 2003.

Plasmids and reagents

Expression constructs for p53R175H, p53R273H, TAp63α, ΔNp63α, TAp63γ and ΔNp63γ, ca TGFβRI, β-gal and Flag-Smad2 were as previously described (Cordenonsi et al., 2003; Dupont et al., 2005). Phosphomutant hp53R175H in N-terminal Ser/Thr sites targeted by Ras/CK1 signaling was generated as previously described (Cordenonsi et al., 2007). Expression vectors for mutant-p53 alleles Y220C, R248W, C277Y and D281G were gifts from C. Prives and G. Blandino (Gaiddon et al., 2001; Strano et al., 2002). The retroviral ΔNp63α expression construct (pBABE- ΔNp63α) was a gift of Leif W. Ellisen (Carroll et al., 2006).

Small-hairpin-RNA (shRNA) expression constructs were generated by cloning annealed DNA oligonucleotides in pSUPER-retro-puro (OligoEngine). A list of the sequences targeted by shRNAs is provided in Table S1. For reconstitution assays, siRNA-insensitive human mutant-p53R175H was custom synthesized from Origene and cloned in lentiviral vector (pRRLsin.ppts.hCMV, gift from L. Naldini). For reconstitution with wild-type p53, we subcloned the mouse-p53 cDNA, insensitive to our anti-hp53 shRNA (Cordenonsi et al., 2007), in the same lentiviral vector. All plasmids were controlled by sequencing. The TGFβRI inhibitor SB431542 and the MEK inhibitor PD98059 were purchased from Tocris and Calbiochem, respectively. TGFβ1 was purchased from Preprotech.

Cell cultures and Transfections

H1299 non-small lung carcinoma cells were maintained in DMEM, 10% serum, 1 mM glutamine. TGFβ treatments were done in DMEM 0.2% serum. Wild-type p53 and p53R175H H1299 cells

express stably transfected plasmids coding for ponasterone-inducible cDNAs for human wild-type or mutant p53R175H alleles, respectively. p53 expression was induced by incubating cells with Ponasterone-A (Alexis, 3 μM) for 16 hours before treatments. MDA-MB-231 were maintained in a 1:1 mixture of DMEM and F12 (DMEM/F12) supplemented with 10% serum, 2 mM glutamine. For TGFβ treatments cells were serum starved for 24 hours and then treated with TGFβ1 (5 ng/ml) in DMEM/F12 without serum. HACAT cells were maintained in DMEM, 10% serum, 2mM glutamine. TGFβ1 and Activin treatments were performed in the same medium. B9 squamous carcinoma cells and D3 and D3S2 spindle carcinoma cells were maintained in DMEM, 10% serum, 2 mM glutamine, non essential aminoacids (Invitrogen); TGFβ1 (5 ng/ml) was added to the same medium. MEFs were generated from 13.5 dpc embryos of the appropriate genotypes and maintained in DMEM supplemented with 10% serum, 2 mM glutamine.

For siRNA transfection, dsRNA oligos (10 picomoles/cm^2) were transfected using the RNAi Max reagent (Invitrogen). A complete list of siRNAs is provided in Table S1. For transient overexpression studies, p63 expression vectors (0.4 ug/cm^2) were transfected in MDA-MB-231 using LT1 reagent (MIRUS). Wild-type and mutant-p53 expression constructs (7.5 ng/cm^2) were transfected in H1299 cells with Lipofectamine 2000 (Invitrogen).

Luciferase assays

Luciferase reporters (25 ng/cm^2) were co-transfected with β-galactosidase (100 ng/cm^2) for normalization. For experiments in Figures 5C and 5D, TAp63α expression construct (75 ng/cm^2) was transfected alone or in combination with mutant-p53 expression constructs using Lipofectamine 2000 (Invitrogen). TGFβ stimulation was provided by cotransfected constitutive active Type 1 TGFβ Receptor (ca TGFβR1, 60 ng/cm^2) and Flag-Smad2 (12.5 ng/cm^2).

Generation of stable cell lines

For stable knock-down, retroviral particles were obtained by transfecting plasmids for expression of shRNAs (pSuperRetro) and VSV envelope in 293gp (gift from M. Tripodi) with calcium-phosphate. Two days after transfection, surnatants were collected, filtered and used to infect of MDA-MB-231. After selection for puromycin resistance, transduced cells were verified for downregulation of the target protein. Lentiviral vectors coding for wild-type-p53, mutant-p53 or p63DD were transfected in 293 cells in combination with pMDG and pCMV8.74 (gifts from L. Naldini) to obtain viral particles used to infect mutant-p53 depleted MDA-MB-231. D3S2-p63 were obtained by retroviral infection of D3S2 with pBABE-ΔNp63α. Cells were drug selected to enrich for positive transfectants. MEFs were infected with a retroviral vector containing activated H-RasG12V cDNA and puromycin resistance as described in Lang et al., 2004.

Histology and immunohistochemistry

Tissues for histological examination were fixed in 4% buffered formalin, dehydrated and embedded in paraffin by standard methods. For counting the total number of independent lesions per lung after tail vein injection, serial sections of the lungs, cut at a distance of 70 um from each other, were stained with Hematoxylin and Eosin. For the experiments depicted in Figures 2E-F, serial sections of the lungs, cut at a distance of 150 um from each other, were first stained with Hematoxylin and Eosin (H&E) and then processed for human cytokeratin expression. Immunohistochemical staining was performed using an indirect immunoperoxidase technique (Bond Polymer Refine Detection; Vision BioSystems, UK). Sections mounted on silanized slides were dewaxed in xylene, dehydrated in ethanol, boiled in 0.01 M citrate buffer (pH 6.0) for 20 min. in a microwawe oven and then incubated with 3% hydrogen peroxide for 5 min. After washing with PBS, they were incubated in 10% normal BSA for 5 min, followed by incubation for 45 min. with monoclonal mouse anti-human Cytokeratin, clone MNF116 (Dako) or anti-Human Von Willebrand Factor polyclonal antibody (Dako). After washing, sections were incubated with labelled polymer (Bond Polymer Refine Detection) and diaminobenzidine. The sections were then counterstained with hematoxylin, dehydrated, cleared, and mounted.

Antibodies and Western Blotting

Western blot analysis was performed as previously described (Piccolo et al., 1999). Briefly, proteins were resolved in 10% NuPage gels (Invitrogen) and transferred to ImmobilonP membranes (Millipore). Chemiluminescence was revealed using SupersignalWest-pico and -dura HRP substrates (Pierce). Anti-human p53 DO-1 and anti-p63 4A4 monoclonal antibodies, and anti-Lamin and HRas polyclonal antibodies were purchased from Santa Cruz biotechnology. Anti-$p21^{WAF1}$ and anti-Smad2/3 monoclonal antibodies were from BD Biosciences. Anti-phospho-Smad3 and anti-Smad2/3 polyclonal antibodies, and anti-mouse p53 1C12 monoclonal antibody were from Cell Signaling. p63 in Figure 5A was purified by immunoprecipitation using a 1:1 mixture of p63 polyclonal antibodies (H-137 and H-129 from Santa Cruz biotechnologies). The analysis of mutant-p53 phosphorylation was carried out by western-blot after immunopurification of endogenous p53. p53 was immunoprecipitated from MDA-MB-231 lysates in binding buffer (20 mM Hepes pH 7.8, 100 mM KCl, 5% Glycerol, 2.5 mM $MgCl_2$, 0.1% NP40) using DO-1 beads (Santa Cruz biotechnology), for 16 hours at 4°C. After three washes in binding buffer, p53 was eluted with acidic buffer (100 mM Glycine, pH 2, 0.1% Np40). After neutralization with 1M Tris pH 8.0 and overnight dialysis against BC100 (20 mM Tris ph7.8, 100 mM NaCl, 10 % Glycerol, 1mM DTT) the purified p53 protein was analyzed by western-blot with phospho-specific anti-Phospho-Ser6 and

anti-Phospho-Ser9 p53 antibodies (Cell Signaling) as previously described (Cordenonsi et al., 2007).

Northern blotting

Total RNA was extracted from cells plated in 6 cm dishes with Trizol (Invitrogen). 10 μg of total RNA per sample were loaded and separated in a 6% formaldehyde/ 1% agarose gel, blotted by upward capillary transfer onto GeneScreenPlus (PerkinElmer) and UV crosslinked. Membranes were pre-hybridized 5 hrs at 42°C with ULTRAhyb-Oligo solution (Ambion), and hybridized with ^{32}P-labeled DNA probes o.n. at 42°C. Membranes were washed at 68°C with 2xSSC/0,5%SDS solutions and exposed for autoradiography. All probes were obtained by random-primer amplification. Sharp-1, Cyclin G2 and Follistatin probe templates were obtained from RZPD EST (HU3_p983B0120D, HU3_p983D0140D2 and RZPD EST HU3_p983D0113D2 respectively). GPR87 and ADAMTS9 probes were obtained cloning RT-PCR products. All probes were validated by sequencing.

q-PCR and RT-PCR

Poly(A)$^+$-RNA was retrotranscribed with M-MLV Reverse Transcriptase (Invitrogen) and oligo-d(T) primers following total RNA purification with Trizol (Invitrogen). Realtime PCR for Sharp-1 and GAPDH were performed on a RotorGene 3000 (Corbett) using FastStart TaqMan Probe Master (Roche) with Roche internal fluorescent probes (UPL#62 and #60 respectively). The Roche system failed to amplify Cyclin G2 products. Thus, Real-time PCR for Cyclin G2 and GAPDH were done by using 7500 Real-Time PCR System (Applied Biosystems) with DyNAmo HS SYBR Green (Finnzymes). Standard RT-PCR were performed as described in Cordenonsi et al., 2003. A list of all PCR primers is provided as Table S2.

Chromatin Immunoprecipitation

Subconfluent MDA-MB-231 and H1299 cells were cultivated in 60 cm^2 dishes and fixed with 1% formaldehyde at room temperature for 10 minutes. After a brief washing in cold PBS, the reaction was blocked by the addiction of glycine at a final concentration of 0.125M for 5 minutes at room temperature. The cells were rinsed with cold PBS and scraped in 2 ml of PBS complemented with protease inhibitors (Roche). The medium was removed after 10 minutes centrifugation at 4°C at 3000 rpm. Cells were swelled twice in 5 volumes of Lysis Buffer (5mM Pipes, 85 mM KCl, 0.5% NP-40, pH8), incubation on ice for 10 minutes and then recovering with centrifugation at 3000 rpm for 5 minutes at 4°C. The resulting nuclei were resuspended and sonicated in sonication buffer (Upstate) Diagenode Bioruptor 200 (High Power, 30 seconds on/off cycles, 5 minutes total time) in

order to have an average genomic DNA fragments length of 1500 bp. Debris were removed by centrifugation, and chromatin was. The chromatin solutions were diluted 10 times in ChIP dilution buffer (Upstate) and pre-cleared for 15 minutes at 4°C with the addiction of 30 ul of 50% slurry proteinA-Sepharose CL4B (GE Healthcare) previously blocked overnight with 1 μg/μl sheared salmon sperm DNA and 1 μg/μl BSA. Precleared chromatin was incubated overnight at 4°C with 5 ug of the specific antibody. Dynabeads protein A beads (Invitrogen, 20 μl/sample) were preblocked overnight with 1 μg/μl sheared salmon sperm DNA and BSA 0.5% in PBS and then resuspended in Chip Dilution Buffer and added to each sample to recover the protein/DNA complexes. After 15 minutes of rotation at 4°C, the beads were collected using DynaMag (Invitrogen) and briefly washed 4 times for each of the following buffers at room temperature: Low Salt, High Salt and LiCl Buffers (from Upstate), and finally in TE buffer. The beads were then resuspended in 30 ul of TE buffer and Protein-DNA complexes were eluted from the beads by incubating the samples with 400 μl of Elution Buffer (1% SDS in TE) at 65°C for 30 minutes. The eluted chromatin was moved to new tubes and the crosslink was reverted by addiction of NaCl to a final concentration of 200 mM and incubation overnight at 65°C. Each solution was then digested with 20 μg of proteinase-K for 1 hr and the DNA extracted by phenol/chlorophorm purification followed by ethanol precipitation with 15 μg of Glycoblue (Ambion). The purified DNA was resuspended in 50 μl of nuclease free water and 2 μl of each sample was used as template for PCR analysis with ExTaq (Takara) according to manufacturer protocol. The resulting PCR are normalized according to the Input of each sample.

Genomic p63 binding element identification

In order to identify the *in vivo* binding site of p63 on *Cyclin G2* genomic region we analyzed a 30 Kb genomic region centered on *Cyclin G2* first exon with p53MH algorithm (http://www.genemapping.cn/p53MH.htm), the candidate sites were then screened by ChIP for specific binding of p63 in MDA-MB-231 cells. Cells were transfected with control- or anti-p63 siRNAs and lysates were analysed by ChIP on candidate sites. By comparing amplicons from control and p63-depleted cells, we identified a p63-element in the second intron.

Microarray analysis

MDA shGFP and shp53 cells were serum-starved for 24 hours, and then either left untreated or treated with TGFβ1 (5 ng/ml for 3 hours) in DMEM/F12 without serum. Four replicas were prepared for each of the four conditions (untreated shGFP, TGFβ- treated shGFP, untreated shp53, TGFβ-treated shp53), for a total of 16 samples. Total RNA was extracted using Trizol (Invitrogen) according to the manufacturer's instructions. Sample preparation for microarray hybridization was

carried out as described in the Affymetrix GeneChip® Expression Analysis Technical Manual. Briefly, 15 μg of total RNA were used to generate double-stranded cDNA (Invitrogen). Synthesis of Biotin-labeled cRNA was performed using the BioArrayTM HighYieldTM RNA Transcript Labeling Kit (ENZO Biochem, New York, NY). The length of the cRNA fragmentation was confirmed using the Agilent 2100 Bioanalyzer (Agilent Technologies). Four biological mRNA replicates for each group were hybridized on Affymetrix GeneChip Human Genome HG-U133 Plus 2.0 arrays. All data analyses were performed in R using Bioconductor libraries and R statistical packages (http://www.r-project.org/, R Development Core Team, 2008). Specifically, BioConductor packages *affyQCReport* and *AffyPLM* were used for standard Affymetrix quality-control procedures. Probe level signals have been converted to expression values using robust multi-array average procedure *rma* (Irizarry et al., 2003). In RMA, PM values have been background adjusted, normalized using quantile normalization, and expression measure calculated using median polish summarization. RMA data with a standard deviation lower than the mean standard deviation of all log signals in all arrays (e.g., 0.2) have been filtered out. The filtered data set resulted in 22644 probesets used for further analysis. Differentially expressed genes have been identified using Significance Analysis of Microarray *samr* (Tusher et al., 2001). SAM is a statistical technique for finding significant genes in microarrays while controlling the False Discovery Rate (FDR). SAM uses repeated permutations of the data to determine if the expression level of any genes is significantly related to the physiological state and the significance is quantified in terms of q-value (Storey, 2002), i.e. the lowest False Discovery Rate at which a gene is called differentially expressed.

Identification of TGFβ target genes

To identify genes whose expression is modified by TGFβ, we compared the expression profile of TGFβ treated MDA-MB-231 cells (either shGFP or shp53) with their untreated controls and selected those transcripts whose q-value was ≤0.1. This selection was further refined setting the lower limit for TGF_ fold induction (or reduction) to 1.5. Using this combined filter, we were able to identify 447 genes differentially regulated between the untreated and TGFβ treated MDA-MB-231 samples. Differentially expressed genes were functionally classified according to DAVID (http://david.abcc.ncifcrf.gov/), the Kyoto Encyclopedia of Genes and Genomes (KEGG; http://www.genome.jp/kegg/) and NCBI Gene databases (NCBI; http://www.ncbi.nlm.nih.gov/sites/entrez?db=gene). Out of 292 genes associated with known functions, 147 genes were reported to be involved in cellular movements, invasive processes and metastasis ("invasive program"). Genes that were regulated by TGFβ1 in a mutant-p53 dependent

manner were identified as those displaying a significant regulation by TGFβ in shGFP, but not in p53-depleted cells (q-value≤0.1). The resulting 5 genes were validated by Northern blot analysis.

Breast cancer datasets

To evaluate the prognostic value of Sharp-1 and Cyclin G2, we collected 6 different datasets (Table 1). For each data set, we performed survival analysis to test if the *minimal signature* could classify patients into clinically distinct groups. Each dataset has been processed independently from the other to preserve the original differences among the various studies (e.g., patient cohort, microarray type, sample processing protocol, etc.). We downloaded breast cancer gene expression datasets with clinical information from Gene Expression Omnibus (http://www.ncbi.nlm.nih.gov/GEO/), Stanford Microarray Database (http://genome-www5.stanford.edu/), or author's individual web pages (http://microarray-pubs.stanford.edu/wound_NKI/explore.html). Table 1 reports the complete list of datasets and their sources. With the exception of EMC, MSK and NKI studies, raw data (e.g., CEL files) were available for all samples. Detailed clinical information could be acquired for any analyzed sample. The datasets included both Affymetrix and dual-channel cDNA microarray platforms. Since all Affymetrix data were from the same HG-U133A platform, no method was needed to map probesets across various generations of Affymetrix GeneChip arrays. When CEL files were available, expression values were generated from intensity signals using the RMA algorithm; values have been background adjusted, normalized using quantile normalization, and expression measure calculated using median polish summarization. In the case of EMC, MSK and NKI studies, data were used as downloaded. Specifically, in the EMC and MSK datasets expression values were calculated using Affymetrix MAS 5.0 algorithm. In Affymetrix HG-U133A array, Cyclin G2 is represented by 3 probesets (202769_at, 202770_s_at, and 211559_s_at), while Sharp-1 is interrogated only by probeset 221530_s_at. The Agilent, Rosetta Inpharmatics array used for the NKI dataset has two probes (Contig2710_RC and Contig50565) for Sharp-1 and a single probe for Cyclin G2.

***Minimal signature* classification**

To identify two groups of samples with either high or low simultaneous expression scores of Sharp1 and Cyclin G2, we defined a classification rule based on summarizing the standardized expression levels of Sharp1 and Cyclin G2 into a combined score with zero mean. Tumors are then classified as *minimal signature Low* if the combined score is negative and as *minimal signature High* if the combined score is positive:

$$minimal\ signature\ Low \rightarrow \frac{x_i^{Sharp-1} - \hat{\mu}^{Sharp-1}}{\hat{\sigma}^{Sharp-1}} + \frac{x_i^{CyclinG2} - \hat{\mu}^{CyclinG2}}{\hat{\sigma}^{CyclinG2}} \leq 0$$

$$minimal\ signature\ High \rightarrow \frac{x_i^{Sharp-1} - \hat{\mu}^{Sharp-1}}{\hat{\sigma}^{Sharp-1}} + \frac{x_i^{CyclinG2} - \hat{\mu}^{CyclinG2}}{\hat{\sigma}^{CyclinG2}} > 0$$

where $x_i^{Sharp-1}$, $x_i^{CyclinG2}$ are the expression levels of Sharp-1 and Cyclin G2 in sample *i* and $\hat{\mu}^{Sharp-1}$, $\hat{\mu}^{CyclinG2}$, $\hat{\sigma}^{Sharp-1}$ and $\hat{\sigma}^{CyclinG2}$ are the estimated means and standard deviations of Sharp-1 and Cyclin G2 calculated over the entire dataset.

This classification was applied for Stockholm, NCI and Uppsala studies based on expression values obtained from RMA, whereas for EMC and MSK expression values have been used as downloaded. In the case of EMC dataset, expression data have been log_2-transformed. In the case of the NKI dataset, to determine an appropriate threshold of the combined score, we used the clinical parameters to quantify the mean combined score of patients with good clinical outcome, i.e. lymph node negative patients who remained free of distant metastases after at least 5 years of follow-up (procedure described in van't Veer et al., 2002). About 30% of the samples met these criteria (89 out of 295 tumors), and the mean combined score values (i.e. 0.4427) was used as the cut-off to classified tumors in either *High* or *Low* groups: if the combined score of a given sample was higher than 0.4427, then the sample was termed *minimal signature High*, otherwise, it was termed *minimal signature Low*. Among the 295 patients, 117 had a *minimal signature High* and 178 a *minimal signature Low*. Samples were also classified into the *minimal signature High* and *minimal signature Low* groups based on the expression levels of Sharp-1 and Cyclin G2 using unsupervised clustering techniques (Kaufman and Rousseeuw, 1990). In particular, agglomerative clustering with Euclidean distance and complete or Ward's linkage criteria has been used for the classification of MSK and EMC datasets, respectively; divisive clustering with Euclidean distance (diana) has been applied to the NCI samples and the k-means partitioning algorithm (Hartigan and Wong, 1979) has been used for the Stockholm and Uppsala datasets. We compared the performance of the *minimal signature* and of the 70-genes signature for all the analyzed dataset. Since all dataset other than NKI are from Affymetrix arrays, we first mapped genes of the 70-genes signature to Affyemtrix probestes, obtaining that the NKI 70-gene poor prognosis signature maps to 75 probesets in the Affymetrix U133A platform corresponding to 48 unique EntrezGene IDs. Given this reduction on the number of genes making up the signature and given the fact that we used a different model for classifying patients, we verified if the prognostic performance of a different model (i.e., an unsupervised clustering) constructed on a reduced gene list is similar to that of van't Veer's model based on the full signature. Thus, we classified NKI samples using the 48 unique genes that are present on both

Affymetrix and Rosetta platforms and a classification model based on unsupervised clustering. In agreement to what previously reported by van't Veer et al., 2002 and by Minn et al., 2005, we found that using an unsupervised clustering on a reduced signature had little impact on the performance of the classifier. Thus, samples in all other data sets have been classified into two groups using this reduced 70-gene signature and unsupervised clustering. In particular, an agglomerative hierarchical model based on Ward's algorithm (Ward, 1963) was used for the Stockholm study, the Uppsala and ECM studies were classified using PAM algorithm (Kaufman and Rousseeuw, 1990). Finally, for MSK study, we used the classification given by Minn et al, 2005.

Survival analysis

To evaluate the prognostic value of the *minimal signature*, we estimated, using the Kaplan-Meier method (Kalbfleisch and Prentice, 1980), the probabilities that patients would remain free of metastases (MSK and NKI), free of tumor recurrence (Stockholm and NCI), and free of cancer disease (Uppsala) according to whether they belong to *High* or *Low* group. To confirm these findings, the survival curves were compared using the log-rank or Mantel-Haenszel test (Harrington and Fleming, 1982), i.e. testing the null hypothesis of no difference against the one-sided alternative supporting *minimal signature High* survival. P-values were calculated according to the standard normal asymptotic distribution and adjusted according to sequential Bonferroni-Holm multiple test procedure (Holm, 1979) to control the family-wise error rate. All the adjusted pvalues were significant at a level _=0.05 when comparing *minimal signature High* and *minimal signature Low* groups as defined using the combined score. The same survival analysis repeated on *minimal signature High* and *minimal signature Low* groups as defined using the clustering techniques returned similar results, with p-values of Stockholm: 0.00026, NCI: 0.00083, EMC: 0.0251, Uppsala: 0.0025, MSK: 0.00887. Finally, the survival analysis was applied to subsets of samples assigned to *High* and *Low* groups and classified as intermediate (grade 2) by the Nottingham scale. Again, all null hypotheses was rejected controlling the family-wise error rate at α=0.05. In the case of the NCI dataset, this analysis could not be performed since the recurrence-free survival curve for grade 2 tumors is not statistically different from the curve of poorly differentiated grade 3 tumors. Information for the Nottingham scale classification of the tumors is not available in the MSK and EMC datasets.

Multivariate analysis using a Cox proportional-hazards model

The analysis of the risk of recurrence for the 187 tumors from the NCI study was conducted using Cox proportional-hazards regression modeling. In particular, we examined the relationship between

survival and the *minimal signature* predictor and other predictors commonly used in the clinical practice, including tumor diameter, estrogenreceptor status (positive vs. negative), nodal status (positive vs. negative), tumor grade (grade 2 vs. grade 1 and grade 3 vs. grade 1) and treatment status (tamoxifen vs. none). We fitted Cox proportional-hazards regression model first by using clinical variables only (Model 1), and then adding the *minimal signature* predictor (Model 2). Survival data from the NKI study of 295 patients with 88 distant metastasis as first event and 207 censored observations was investigated. Available clinical predictors are: tumor diameter (> 2 cm vs. <= 2 cm), estrogen-receptor status (positive vs. negative), no. of positive nodes (1-3 vs. 0 and >=4 vs. 0), tumor grade (grade 2 vs. grade 1 and grade 3 vs. grade 1), mastectomy (yes vs. no), hormonal treatment (yes vs. no) and chemotheraphy (yes vs. no). We fitted Cox proportional-hazards regression model first by using clinical variables only (Model 1), and then adding the *minimal signature* predictor (Model 2). For both analysis, we determined whether the fitted Cox regression model adequately describes the data by considering diagnostics for violation of the assumptions. Tests and graphical diagnostics were applied, but no evidence was found (see http://www.mayo.edu/hsr/people/therneau/survival.ps for further detail.

BIBLIOGRAPHY

Albini, A. (1998). Tumor and endothelial cell invasion of basement membranes. The matrigel chemoinvasion assay as a tool for dissecting molecular mechanisms. Pathol Oncol Res *4*, 230-241.

Arteaga, C.L., Hurd, S.D., Winnier, A.R., Johnson, M.D., Fendly, B.M., and Forbes, J.T. (1993). Anti-transforming growth factor (TGF)-beta antibodies inhibit breast cancer cell tumorigenicity and increase mouse spleen natural killer cell activity. Implications for a possible role of tumor cell/host TGF-beta interactions in human breast cancer progression. J Clin Invest *92*, 2569-2576.

Bandyopadhyay, A., Zhu, Y., Cibull, M.L., Bao, L., Chen, C., and Sun, L. (1999). A soluble transforming growth factor beta type III receptor suppresses tumorigenicity and metastasis of human breast cancer MDA-MB-231 cells. Cancer Res *59*, 5041-5046.

Barbieri, C.E., and Pietenpol, J.A. (2006). p63 and epithelial biology. Experimental cell research *312*, 695-706.

Bernards, R., and Weinberg, R.A. (2002). A progression puzzle. Nature *418*, 823.

Biswas, S., Criswell, T.L., Wang, S.E., and Arteaga, C.L. (2006). Inhibition of transforming growth factor-beta signaling in human cancer: targeting a tumor suppressor network as a therapeutic strategy. Clin Cancer Res *12*, 4142-4146.

Carroll, D.K., Carroll, J.S., Leong, C.O., Cheng, F., Brown, M., Mills, A.A., Brugge, J.S., and Ellisen, L.W. (2006). p63 regulates an adhesion programme and cell survival in epithelial cells. Nat Cell Biol *8*, 551-561.

Caulin, C., Nguyen, T., Lang, G.A., Goepfert, T.M., Brinkley, B.R., Cai, W.W., Lozano, G., and Roop, D.R. (2007). An inducible mouse model for skin cancer reveals distinct roles for gain- and loss-of-function p53 mutations. J Clin Invest *117*, 1893-1901.

Cordenonsi, M., Dupont, S., Maretto, S., Insinga, A., Imbriano, C., and Piccolo, S. (2003). Links between tumor suppressors: p53 is required for TGF-beta gene responses by cooperating with Smads. Cell *113*, 301-314.

Cordenonsi, M., Montagner, M., Adorno, M., Zacchigna, L., Martello, G., Mamidi, A., Soligo, S., Dupont, S., and Piccolo, S. (2007). Integration of TGF-beta and Ras/MAPK signaling through p53 phosphorylation. Science *315*, 840-843.

Cui, W., Fowlis, D.J., Bryson, S., Duffie, E., Ireland, H., Balmain, A., and Akhurst, R.J. (1996). TGFbeta1 inhibits the formation of benign skin tumors, but enhances progression to invasive spindle carcinomas in transgenic mice. Cell *86*, 531-542.

Dadiani, M., Kalchenko, V., Yosepovich, A., Margalit, R., Hassid, Y., Degani, H., and Seger, D. (2006). Real-time imaging of lymphogenic metastasis in orthotopic human breast cancer. Cancer Res *66*, 8037-8041.

Deckers, M., van Dinther, M., Buijs, J., Que, I., Lowik, C., van der Pluijm, G., and ten Dijke, P. (2006). The tumor suppressor Smad4 is required for transforming growth factor beta-induced epithelial to mesenchymal transition and bone metastasis of breast cancer cells. Cancer Res *66*, 2202-2209.

Derynck, R., Akhurst, R.J., and Balmain, A. (2001). TGF-beta signaling in tumor suppression and cancer progression. Nat Genet *29*, 117-129.

Deyoung, M.P., and Ellisen, L.W. (2007). p63 and p73 in human cancer: defining the network. Oncogene *26*, 5169-5183.

Dupont, S., Zacchigna, L., Adorno, M., Soligo, S., Volpin, D., Piccolo, S., and Cordenonsi, M. (2004). Convergence of p53 and TGF-beta signaling networks. Cancer Lett *213*, 129-138.

Dupont, S., Zacchigna, L., Cordenonsi, M., Soligo, S., Adorno, M., Rugge, M., and Piccolo, S. (2005). Germ-layer specification and control of cell growth by Ectodermin, a Smad4 ubiquitin ligase. Cell *121*, 87-99.

Elston, C.W., and Ellis, I.O. (1991). Pathological prognostic factors in breast cancer. I. The value of histological grade in breast cancer: experience from a large study with long-term follow-up. Histopathology *19*, 403-410.

Fan, C., Oh, D.S., Wessels, L., Weigelt, B., Nuyten, D.S., Nobel, A.B., van't Veer, L.J., and Perou, C.M. (2006). Concordance among gene-expression-based predictors for breast cancer. N Engl J Med *355*, 560-569.

Ferbeyre, G., and Lowe, S.W. (2002). The price of tumour suppression? Nature *415*, 26-27.

Fidler, I.J. (2003). The pathogenesis of cancer metastasis: the 'seed and soil' hypothesis revisited. Nat Rev Cancer *3*, 453-458.

Flores, E.R., Sengupta, S., Miller, J.B., Newman, J.J., Bronson, R., Crowley, D., Yang, A., McKeon, F., and Jacks, T. (2005). Tumor predisposition in mice mutant for p63 and p73: evidence for broader tumor suppressor functions for the p53 family. Cancer Cell *7*, 363-373.

Gaiddon, C., Lokshin, M., Ahn, J., Zhang, T., and Prives, C. (2001). A subset of tumor-derived mutant forms of p53 down-regulate p63 and p73 through a direct interaction with the p53 core domain. Mol Cell Biol *21*, 1874-1887.

Grunert, S., Jechlinger, M., and Beug, H. (2003). Diverse cellular and molecular mechanisms contribute to epithelial plasticity and metastasis. Nat Rev Mol Cell Biol *4*, 657-665.

Gupta, G.P., and Massague, J. (2006). Cancer metastasis: building a framework. Cell *127*, 679-695.

Harrington, D.P., and Fleming, T.R. (1982). A class of rank test procedures for censored survival data. Biometrika *69*, 4.

Hartigan, J.A., and Wong, M.A. (1979). A K-means clustering algorithm. Applied Statistics *28*, 9.

Hingorani, S.R., Wang, L., Multani, A.S., Combs, C., Deramaudt, T.B., Hruban, R.H., Rustgi, A.K., Chang, S., and Tuveson, D.A. (2005). Trp53R172H and KrasG12D cooperate to promote chromosomal instability and widely metastatic pancreatic ductal adenocarcinoma in mice. Cancer Cell *7*, 469-483.

Hoh, J., Jin, S., Parrado, T., Edington, J., Levine, A.J., and Ott, J. (2002). The p53MH algorithm and its application in detecting p53-responsive genes. Proceedings of the National Academy of Sciences of the United States of America *99*, 8467-8472.

Holm, S. (1979). A simple sequentially rejective multiple test procedure. Scandinavian Journal of Statistics *6*, 6.

Irizarry, R.A., Bolstad, B.M., Collin, F., Cope, L.M., Hobbs, B., and Speed, T.P. (2003). Summaries of Affymetrix GeneChip probe level data. Nucleic Acids Res *31*, e15.

Kalbfleisch, J.D., and Prentice, R.L. (1980). The statistical analysis of failure time data (New York ; Chichester, Wiley).

Kaufman, L., and Rousseeuw, P.J. (1990). Finding groups in data : an introduction to cluster analysis (New York ; Chichester, Wiley).

Kleihues, P., Schauble, B., zur Hausen, A., Esteve, J., and Ohgaki, H. (1997). Tumors associated with p53 germline mutations: a synopsis of 91 families. The American journal of pathology *150*, 1-13.

Lang, G.A., Iwakuma, T., Suh, Y.A., Liu, G., Rao, V.A., Parant, J.M., Valentin-Vega, Y.A., Terzian, T., Caldwell, L.C., Strong, L.C*., et al.* (2004). Gain of function of a p53 hot spot mutation in a mouse model of Li-Fraumeni syndrome. Cell *119*, 861-872.

Li, B., Rosen, J.M., McMenamin-Balano, J., Muller, W.J., and Perkins, A.S. (1997). neu/ERBB2 cooperates with p53-172H during mammary tumorigenesis in transgenic mice. Mol Cell Biol *17*, 3155-3163.

Li, Y., and Prives, C. (2007). Are interactions with p63 and p73 involved in mutant p53 gain of oncogenic function? Oncogene *26*, 2220-2225.

Lowe, S.W., Cepero, E., and Evan, G. (2004). Intrinsic tumour suppression. Nature *432*, 307-315.

Lowe, S.W., and Sherr, C.J. (2003). Tumor suppression by Ink4a-Arf: progress and puzzles. Current opinion in genetics & development *13*, 77-83.

Massague, J. (2000). How cells read TGF-beta signals. Nat Rev Mol Cell Biol *1*, 169-178.

Minn, A.J., Kang, Y., Serganova, I., Gupta, G.P., Giri, D.D., Doubrovin, M., Ponomarev, V., Gerald, W.L., Blasberg, R., and Massague, J. (2005). Distinct organ-specific metastatic potential of individual breast cancer cells and primary tumors. J Clin Invest *115*, 44-55.

Muraoka, R.S., Koh, Y., Roebuck, L.R., Sanders, M.E., Brantley-Sieders, D., Gorska, A.E., Moses, H.L., and Arteaga, C.L. (2003). Increased malignancy of Neu-induced mammary tumors overexpressing active transforming growth factor beta1. Mol Cell Biol *23*, 8691-8703.

Murray-Zmijewski, F., Lane, D.P., and Bourdon, J.C. (2006). p53/p63/p73 isoforms: an orchestra of isoforms to harmonise cell differentiation and response to stress. Cell death and differentiation *13*, 962-972.

Oft, M., Akhurst, R.J., and Balmain, A. (2002). Metastasis is driven by sequential elevation of H-ras and Smad2 levels. Nat Cell Biol *4*, 487-494.

Olive, K.P., Tuveson, D.A., Ruhe, Z.C., Yin, B., Willis, N.A., Bronson, R.T., Crowley, D., and Jacks, T. (2004). Mutant p53 gain of function in two mouse models of Li-Fraumeni syndrome. Cell *119*, 847-860.

Padua, D., Zhang, X.H., Wang, Q., Nadal, C., Gerald, W.L., Gomis, R.R., and Massague, J. (2008). TGFbeta primes breast tumors for lung metastasis seeding through angiopoietin-like 4. Cell *133*, 66-77.

Piccolo, S., Agius, E., Leyns, L., Bhattacharyya, S., Grunz, H., Bouwmeester, T., and De Robertis, E.M. (1999). The head inducer Cerberus is a multifunctional antagonist of Nodal, BMP and Wnt signals. Nature *397*, 707-710.

Serber, Z., Lai, H.C., Yang, A., Ou, H.D., Sigal, M.S., Kelly, A.E., Darimont, B.D., Duijf, P.H., Van Bokhoven, H., McKeon, F.*, et al.* (2002). A C-terminal inhibitory domain controls the activity of p63 by an intramolecular mechanism. Molecular and cellular biology *22*, 8601-8611.

Siegel, P.M., and Massague, J. (2003). Cytostatic and apoptotic actions of TGF-beta in homeostasis and cancer. Nat Rev Cancer *3*, 807-821.

Sobin, L.H., Wittekind, C., and International Union against Cancer. (2002). TNM classification of malignant tumours, 6th edn (New York, Wiley-Liss).

Sorlie, T., Perou, C.M., Tibshirani, R., Aas, T., Geisler, S., Johnsen, H., Hastie, T., Eisen, M.B., van de Rijn, M., Jeffrey, S.S.*, et al.* (2001). Gene expression patterns of breast carcinomas distinguish tumor subclasses with clinical implications. Proc Natl Acad Sci U S A *98*, 10869-10874.

Sotiriou, C., Wirapati, P., Loi, S., Harris, A., Fox, S., Smeds, J., Nordgren, H., Farmer, P., Praz, V., Haibe-Kains, B.*, et al.* (2006). Gene expression profiling in breast cancer: understanding the molecular basis of histologic grade to improve prognosis. J Natl Cancer Inst *98*, 262-272.

Soussi, T., and Lozano, G. (2005). p53 mutation heterogeneity in cancer. Biochem Biophys Res Commun *331*, 834-842.

Storey, J.D. (2002). A direct approach to false discovery rates. Journal of the Royal Statistical Society Series B-Statistical Methodology *64*, 479-498.

Strano, S., Fontemaggi, G., Costanzo, A., Rizzo, M.G., Monti, O., Baccarini, A., Del Sal, G., Levrero, M., Sacchi, A., Oren, M.*, et al.* (2002). Physical interaction with human tumor-derived p53 mutants inhibits p63 activities. J Biol Chem *277*, 18817-18826.

Strano, S., Munarriz, E., Rossi, M., Cristofanelli, B., Shaul, Y., Castagnoli, L., Levine, A.J., Sacchi, A., Cesareni, G., Oren, M.*, et al.* (2000). Physical and functional interaction between p53 mutants and different isoforms of p73. J Biol Chem *275*, 29503-29512.

Tusher, V.G., Tibshirani, R., and Chu, G. (2001). Significance analysis of microarrays applied to the ionizing radiation response. Proceedings of the National Academy of Sciences of the United States of America *98*, 5116-5121.

van 't Veer, L.J., Dai, H., van de Vijver, M.J., He, Y.D., Hart, A.A., Mao, M., Peterse, H.L., van der Kooy, K., Marton, M.J., Witteveen, A.T.*, et al.* (2002). Gene expression profiling predicts clinical outcome of breast cancer. Nature *415*, 530-536.

Vijayachandra, K., Lee, J., and Glick, A.B. (2003). Smad3 regulates senescence and malignant conversion in a mouse multistage skin carcinogenesis model. Cancer research *63*, 3447-3452.

Vousden, K.H., and Prives, C. (2005). P53 and prognosis: new insights and further complexity. Cell *120*, 7-10.

Wakefield, L.M., and Roberts, A.B. (2002). TGF-beta signaling: positive and negative effects on tumorigenesis. Current opinion in genetics & development *12*, 22-29.

Ward, J.H. (1963). Hierarchical Grouping to optimize an objective function. Journal of American Statistical Association *301*, 9.

Yang, A., Kaghad, M., Wang, Y., Gillett, E., Fleming, M.D., Dotsch, V., Andrews, N.C., Caput, D., and McKeon, F. (1998). p63, a p53 homolog at 3q27-29, encodes multiple products with transactivating, death-inducing, and dominant-negative activities. Mol Cell *2*, 305-316.

FIGURES

Figure 1. Mutant-p53 expression promotes TGFβ pro-migratory responses

(A) Schematic representation of our starting hypothesis. Wild-type p53 is enabled by RAS to bind Smad2/3 to control the TGFβ growth arrest program (Cordenonsi et al., 2007). The present study was undertaken to test if such physiological pathway is diverted in cancer cells to foster TGFβ invasion, migration and metastasis.

(B) Western blot of H1299 cell lysates: parental, i.e., lacking p53 expression (null), reconstituted with wild-type p53 (p53 wt) or mutant-p53 (p53 R175H). The TGFβ signaling cascade is similarly active in the three cell lines, as monitored by Smad3 phosphorylation (P-Smad3). The CDK inhibitor $p21^{WAF1}$, a marker for TGFβ growth arrest, is activated only in cells reconstituted with wild-type p53. Lamin-B is a loading control.

(C) Effect of TGFβ (5ng/ml of TGFβ for 24 hrs) on the morphology of H1299 cells.

(D) Wound healing assays of H1299 cells showing effect of mutant-p53 on TGFβ driven migration. Pictures were taken 30 hours after scratching the cultures.

(E) H1299 cells were seeded on transwell membranes. When indicated, cells were treated with TGFβ (4 ng/ml). The graph show the number of cells migrated through the transwell after 16 hrs. Only H1299 reconstituted with p53R175H cells acquire the ability to migrate in response to TGFβ.

(F) TGFβ signaling is not affected by mutant-p53 expression. H1299 cells, either null or reconstituted with p53R175H, were transiently transfected with pCAGA12-lux, a reporter for Smad transcriptional activity, and treated with increasing doses of TGFβ. Graphs show luciferase activity after 6 hours of treatment.

Figure 1

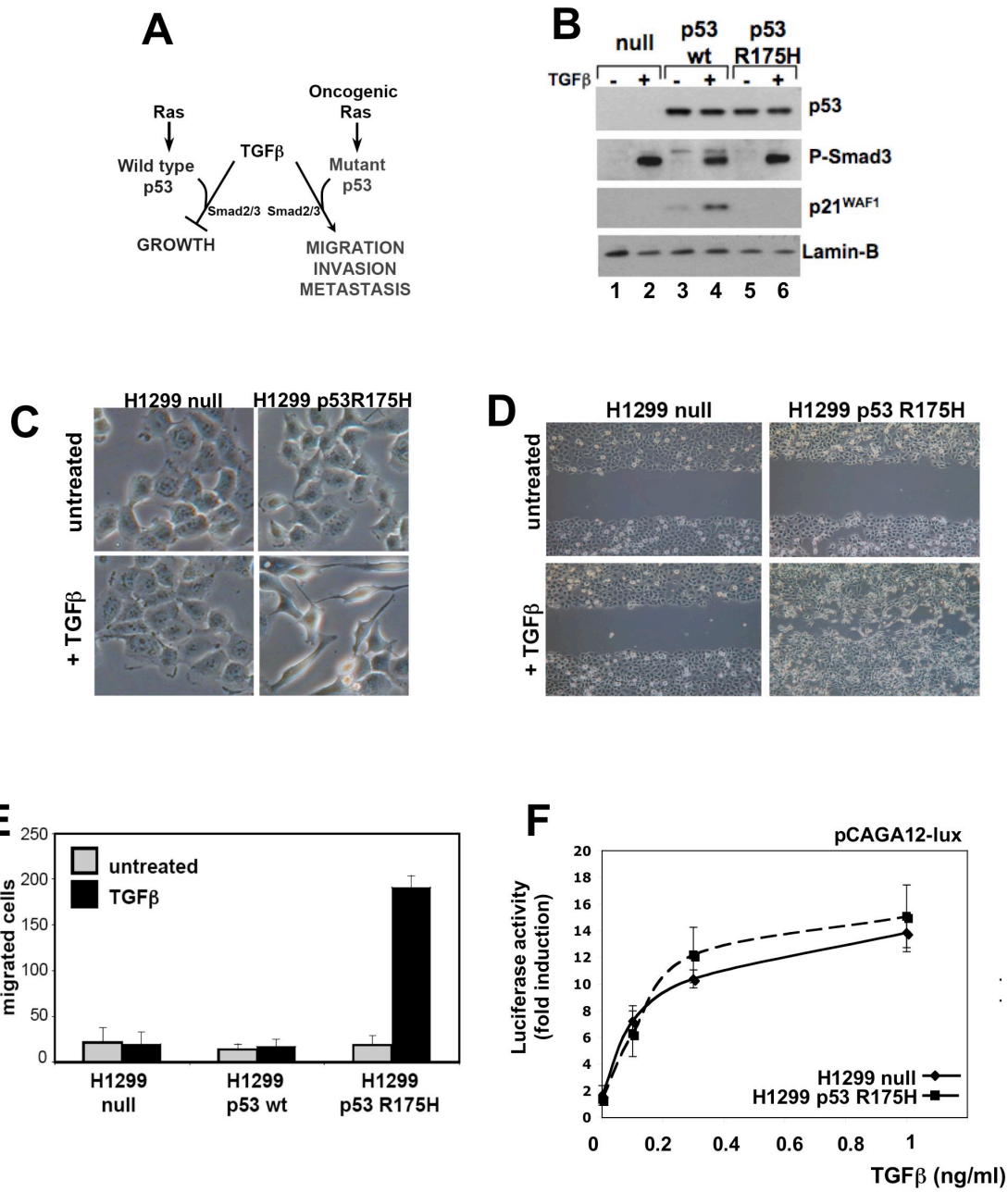
A
Ras
Wild type p53
TGFβ
Smad2/3
GROWTH
Oncogenic Ras
Mutant p53
Smad2/3
MIGRATION INVASION METASTASIS
B
null
p53 wt
p53 R175H
TGFβ
- + - + - +
p53
P-Smad3
p21WAF1
Lamin-B
1 2 3 4 5 6
C
H1299 null
H1299 p53R175H
untreated
+ TGFβ
D
H1299 null
H1299 p53 R175H
untreated
+ TGFβ
E
migrated cells
250
200
150
100
50
0
untreated
TGFβ
H1299 null
H1299 p53 wt
H1299 p53 R175H
F
pCAGA12-lux
Luciferase activity (fold induction)
20
18
16
14
12
10
8
6
4
2
0
0
0.2
0.4
0.6
0.8
1
H1299 null
H1299 p53 R175H
TGFβ (ng/ml)

Figure 2. Mutant-p53 is required for TGFβ-driven invasion and metastasis in breast cancer MDAMB-231 cells

(A) Transwell assay for TGFβ dependent migration of MDA-MB-231 cell lines. TGFβ was used at 5 ng/ml. This response depends on canonical Smad signaling, as attested by blockade of migration ensuing Smad4 depletion (compare lanes 1 and 2). Endogenous mutant-p53 is required for this response as validated by two independent siRNA sequences (A and B, respectively, lanes 3 and 4). The sequence corresponding to siRNA-B was cloned in pSUPER-Retro and used for stable p53 interference. We tested the whole population of positive transfectants (lane 6) or two independent clones (lanes 7 and 8). TGFβ-dependent migration of clone 2 is rescued by infection with a lentiviral vector coding for siRNA-resistant mutant-p53 (R175H, lane 9).

(B and C) SCID mice were injected in the fat pad with MDA shGFP or MDA shp53 cells. (B) The rate of primary tumor growth was similar between the two cell populations. (C) Number of mice scored positive for lymphonodal metastasis. To quantify metastatic spread, we monitored the colonization of controlateral lymph nodes, a read-out of systemic disease in human breast cancers (Sobin et al., 2002).

(D, E and F) Lung colonization assays after tail vein injection of MDA-MB-231 cell lines (1×10^6 cells/mouse). (D) Total number of lung metastatic nodules in individual mice were counted on serial histological sections. Lane 1: control (shGFP) cells (n=20). Lane 2: canonical Smad signaling is required for MDA-MB-231 lung metastasis as revealed by the inhibitory effect of Smad4 depletion (n=9). Lanes 3 and 4: impaired metastasis in two independent shp53 clonal cell lines (clone 1 and 2, siRNA sequence B, see Figure 2A). Clone1, n=10; clone 2, n=21. Similar result was obtained by depletion of mutant-p53 with siRNA sequence A (Figure S2E). Lanes 5 and 6: effect of reconstitution with wild-type (n=10) and mutant-p53 (R175H, n=12). Panels show representative immunohistochemistry for human cytokeratin in sections of lungs from mice injected with MDA shGFP (E) or MDA shp53 (F).

Figure 2

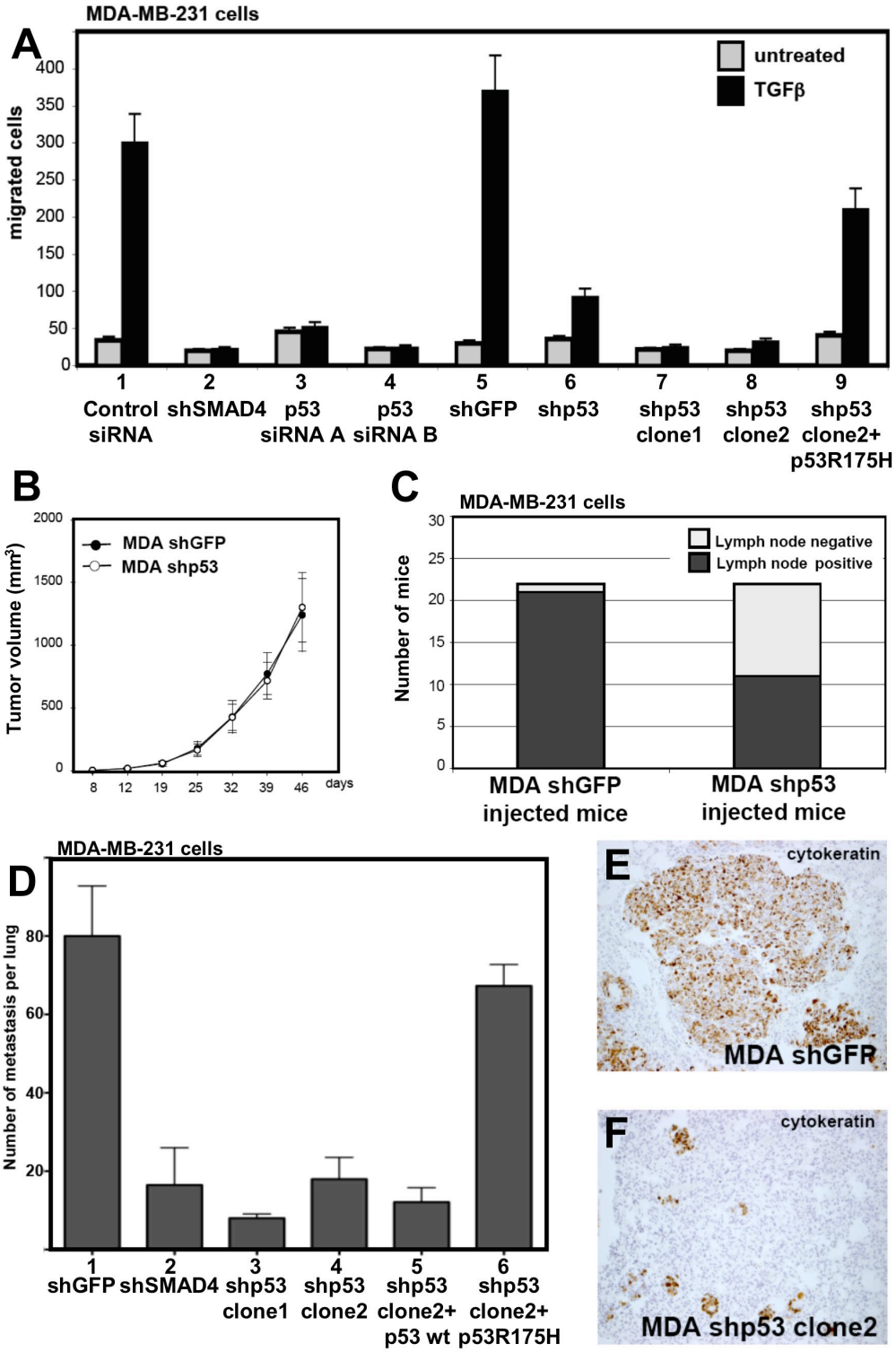
MDA-MB-231 cells
A
migrated cells
untreated
TGFβ
1 Control siRNA
2 shSMAD4
3 p53 siRNA A
4 p53 siRNA B
5 shGFP
6 shp53
7 shp53 clone1
8 shp53 clone2
9 shp53 clone2+ p53R175H
B
Tumor volume (mm³)
MDA shGFP
MDA shp53
days
C
MDA-MB-231 cells
Number of mice
Lymph node negative
Lymph node positive
MDA shGFP injected mice
MDA shp53 injected mice
D
MDA-MB-231 cells
Number of metastasis per lung
1 shGFP
2 shSMAD4
3 shp53 clone1
4 shp53 clone2
5 shp53 clone2+ p53 wt
6 shp53 clone2+ p53R175H
E
cytokeratin
MDA shGFR
F
cytokeratin
MDA shp53 clone2

Figure 3.

(A) Assay for invasive activity of MDA-MB-231 cells embedded in a drop of matrigel. Panels show pictures of the same field at different time points. Dotted lines highlight the edges of the drop. Only control cells are able to evade from the matrigel (arrows). This process is dependent on TGFβϖ signaling as it is blocked by treatment with the TGFβR1 inhibitor SB431542 (5 μM). MDA shp53 cells are impaired in matrix degradation and evasion.

(B) MDA-MB-231 cells display spindle shape in 3D culture conditions, once embedded in matrigel (top panel). Arrowheads indicate lamellipodia protrusions. Conversely, MDA shp53 formed clusters of adherent, cobble-stone shaped cells (bottom panel). Inhibition of TGFβ signaling parallels the phenotypic effects of mutant-p53 depletion (data not shown).

(C) Western blot showing p53 protein depletion in MDA-MB-231 expressing a shRNA targeting p53 (MDA-shp53).

Figure 3

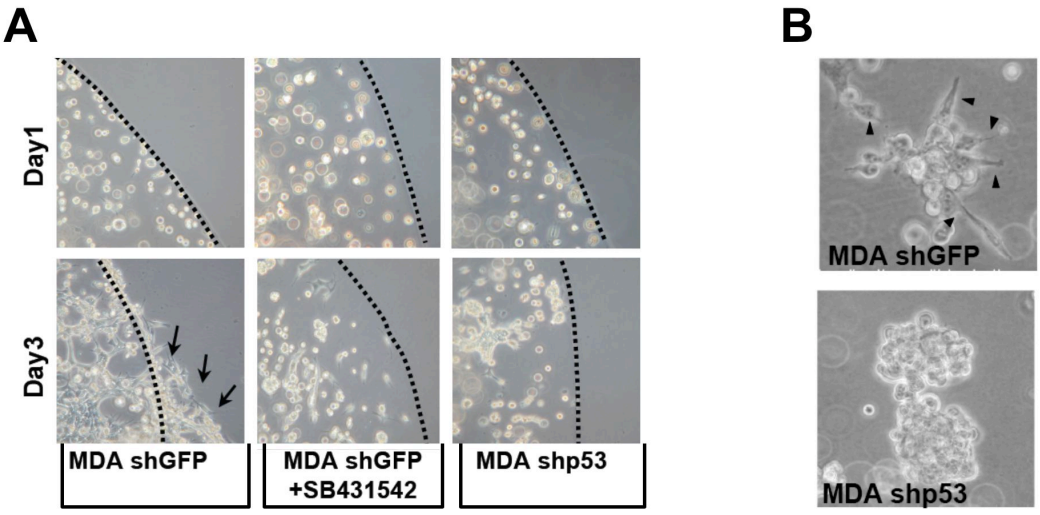
A
Day1
Day3
MDA shGFP
MDA shGFP
+SB431542
MDA shp53
B
MDA shGFP
MDA shp53

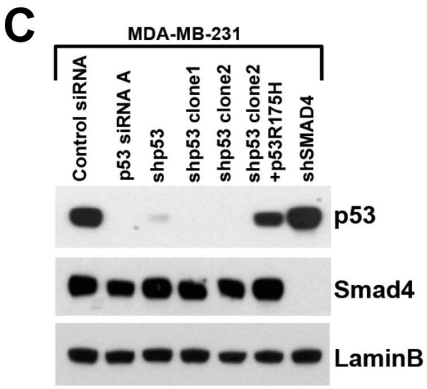
C
MDA-MB-231
Control siRNA
p53 siRNA A
shp53
shp53 clone1
shp53 clone2
shp53 clone2
+p53R175H
shSMAD4
p53
Smad4
LaminB

Figure 4. p63 opposes TGFβ-driven migration

(A) Transwell assay of MDA-MB-231 transiently transfected with the indicated p63 expression vectors.

(B) Loss of p63 confers migratory abilities to H1299 cells in response to TGFβ, phenocopying the gain of mutant-p53. Graphs show quantification of cells migrated into a defined wound area 24 hrs after cell scraping.

(C) Transwell migration assay of MDA-MB-231 after transfection of indicated siRNAs. TGFβ induced migration is impaired by loss of mutant-p53, but is rescued in cells with dual depletion of both p53 and p63. Note that once p63 is depleted, mutant-p53 becomes dispensable - and TGFβ-proficient - for induction of cell migration (see diagram in D).

(D) Model of the epistatic relationships between TGFβ, mutant-p53 and p63.

(E) Functional inactivation of p63 by overexpression of p63DD in shp53MDA-MB-231 clone 2 (as in Figure 2D) rescues lung metastastic colonization in tail vein assays (n=8, 1 x 10^6 cells/mouse.

(F) p63DD expression antagonizes p63 transcriptional activity on the reporter plasmid p53-lux in H1299.

Figure 4

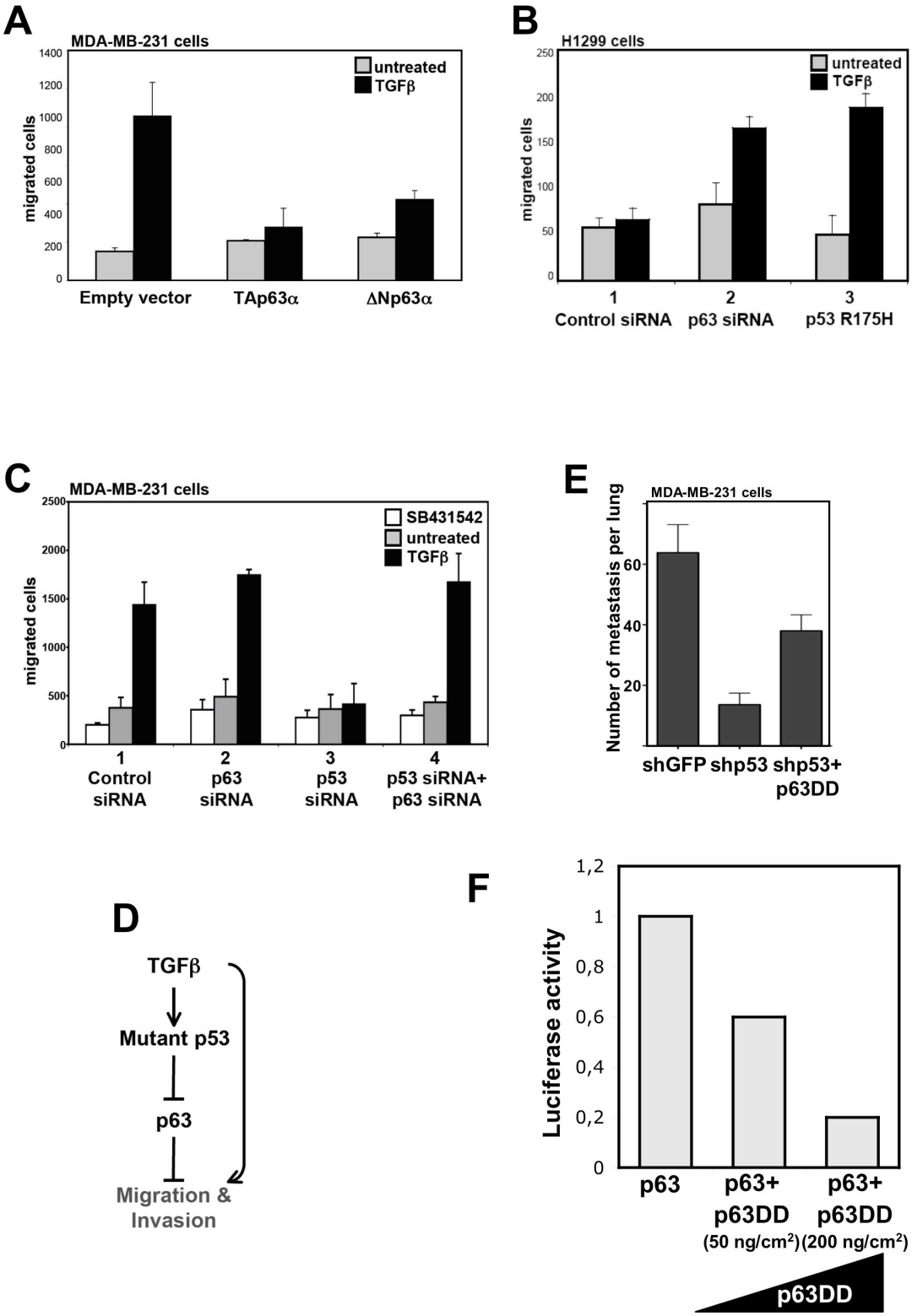
A
MDA-MB-231 cells
migrated cells
untreated
TGFβ
Empty vector
TAp63α
ΔNp63α
B
H1299 cells
migrated cells
untreated
TGFβ
1
Control siRNA
2
p63 siRNA
3
p53 R175H
C
MDA-MB-231 cells
migrated cells
SB431542
untreated
TGFβ
1
Control siRNA
2
p63 siRNA
3
p53 siRNA
4
p53 siRNA+ p63 siRNA
E
MDA-MB-231 cells
Number of metastasis per lung
shGFP
shp53
shp53+ p63DD
D
TGFβ
Mutant p53
p63
Migration & Invasion
F
Luciferase activity
p63
p63+ p63DD (50 ng/cm²)
p63+ p63DD (200 ng/cm²)
p63DD

Figure 5. TGFβ and Ras signaling promote the assembly of a mutant-p53/Smad2/p63 complex

(A) Co-immunoprecipitation/western blot analysis of HACAT cell lysates showing endogenous p63 bound to mutant-p53 Cells were left untreated (lane 2) or treated for 1 hour either with 5 μM SB431542 (lane 1) or with TGFβ 1 (5 ng/ml, lanes 3-5). Cells were transfected with anti-Smad2/3 (lane 4) or anti-p53 (lane 5) siRNAs two days before TGFβ treatment. The amount of p63 protein bound to mutant-p53 is shown as percentage relative to the amount of total p63 in the inputs.

(B) Western blot analysis of endogenous proteins: p63 and mutant-p53 coimmunoprecipitated with Smad2 from HACAT cell lysates.

(C) RAS signaling enables ternary complex formation in MDA-MB-231 cells. Panels show western blot analysis of p53 immunocomplexes from lysates of MDA-MB-231 left untreated (lane 1) or incubated for 1 hour with TGFβ1 (5 ng/ml) (lanes 2-5). p63 and Smad2 copurify with mutant-p53 in a TGFβ dependent manner (lanes 1 and 2). Mutant-p53 interaction with p63 is disrupted in cells depleted of Smad2 and Smad3 (lane 3) or when mutant-p53/Smad interaction is impaired by inhibiting the RAS pathway with PD98059 (lane 4). As specificity control, immunoprecipitations were carried out from p53-depleted cells (lane 5).

(D) The RAS/MEK/CK1δ/ε signaling pathway is required for TGFβ induced cell migration. The graph shows number of MDA-MB-231 cells migrated in a transwell assay. Cell migration in response to TGFβ1 is impaired by treatment with the MEK inhibitor PD98059 (60 μM) or by transfection with anti-CK1δ/ε siRNAs. Similar results were obtained by treating cells with the CK1δ/ε small molecule inhibitor IC-261 (data not shown, Cordenonsi et al., 2007).

(E) Lung colonization after tail vein injection of control and CK1δ/ε-depleted MDA-MB-231 cells (n=10, 3 x 10^5 cells/mouse).

(F) MEK activity is required for mutant-p53 N-terminal phosphorylation. Panels show western blot analysis with anti-phospho-specific antibodies of endogenous mutant-p53 purified from lysates of untreated or PD98059-treated MDA-MB-231 cells. The small molecule inhibitor PD98059 blocks Ras signaling at the level of MEK. As expected from previous work (Cordenonsi et al., 2007), mutant-p53 is phosphorylated at CK1δ/ε consensus sites.

(G) The formation of the endogenous mutant-p53/p63/RSmad complex is inhibited in CK1δ/ε-depleted cells. MDA-MB-231 cells were treated with TGFβ1 or with the TGFβ receptor inhibitor SB431542 (to quench autocrine signaling); lysates were purified on an immobilized anti-p53 antibody and co-purified proteins analyzed by western blot. Arrowhead: aspecific Igg band.

(H) The formation of the mutant-p53/p63/RSmad complex requires N-terminal p53 phosphorylation by Ras/CK1 signaling. H1299 cells were transfected with empty vector, wild-type p53, mutant-p53 (p53R175H) and its N-terminal phosphomutant-derivative or with an independent hot-spot mutant-p53 allele (p53R273H). Cells were treated for 1 hour with TGFβ and extracts immunopurified with anti-p53 antibody. Note how wildtype p53 is unable to induce the formation of the ternary complex.

Figure 5

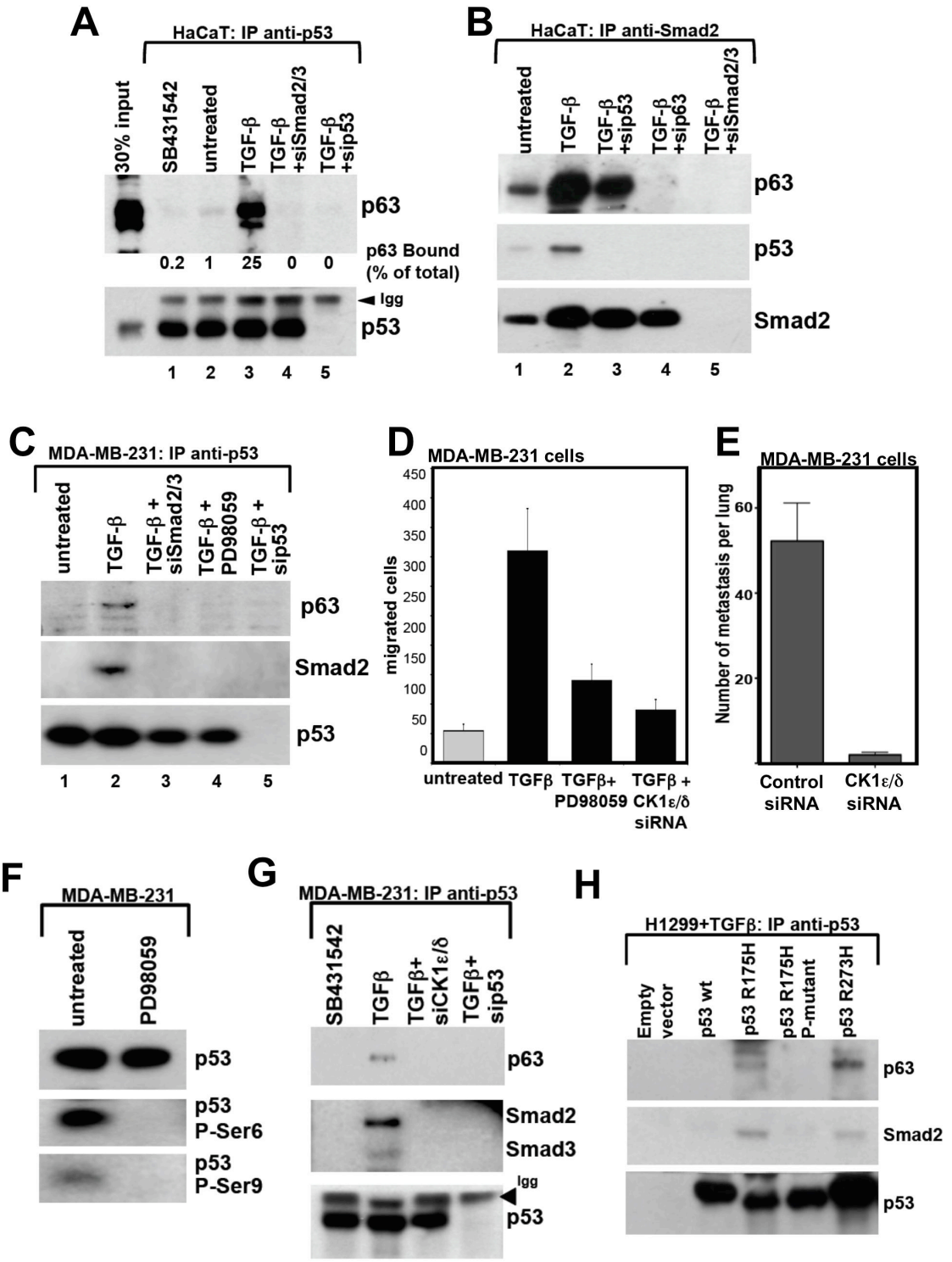
A
HaCaT: IP anti-p53
30% input
SB431542
untreated
TGF-β
TGF-β +siSmad2/3
TGF-β +sip53
p63
p63 Bound (% of total)
0.2 1 25 0 0
Igg
p53
1 2 3 4 5
B
HaCaT: IP anti-Smad2
untreated
TGF-β
TGF-β +sip53
TGF-β +sip63
TGF-β +siSmad2/3
p63
p53
Smad2
1 2 3 4 5
C
MDA-MB-231: IP anti-p53
untreated
TGF-β
TGF-β + siSmad2/3
TGF-β + PD98059
TGF-β + sip53
p63
Smad2
p53
1 2 3 4 5
D
MDA-MB-231 cells
migrated cells
450
400
350
300
250
200
150
100
50
0
untreated
TGFβ
TGFβ+ PD98059
TGFβ + CK1ε/δ siRNA
E
MDA-MB-231 cells
Number of metastasis per lung
60
40
20
Control siRNA
CK1ε/δ siRNA
F
MDA-MB-231
untreated
PD98059
p53
p53 P-Ser6
p53 P-Ser9
G
MDA-MB-231: IP anti-p53
SB431542
TGFβ
TGFβ+ siCK1ε/δ
TGFβ+ sip53
p63
Smad2
Smad3
Igg
p53
H
H1299+TGFβ: IP anti-p53
Empty vector
p53 wt
p53 R175H
p53 R175H P-mutant
p53 R273H
p63
Smad2
p53

Figure 6. Mapping of interaction domains between p63 isoforms and Smad3.

(A) p63 isoforms and domains were *in vitro* transcribed and translated with reticulocytes extracts and incubated with resin-bound GST-tagged Smad3, MH1 and MH2 proteins (sythetized with the same transcription and translation coupled system). p63 and Smad3 have two distinct interaction surfaces: N-terminal TA domain binds Smad3-MH1 domain, C-terminal TI domain of p63 contacts Smad3-MH2. TA: Transcription Activation Domain. DBD: DNA Binding Domain. OD: Oligomerization Domain. QP: Proline-rich Domain. SAM: Sterile α-motif. TID: Transcription Inhibition Domain.

(B) Model for the ternary complex between ΔNp63α, Smad2 and mutant-p53.

Figure 6

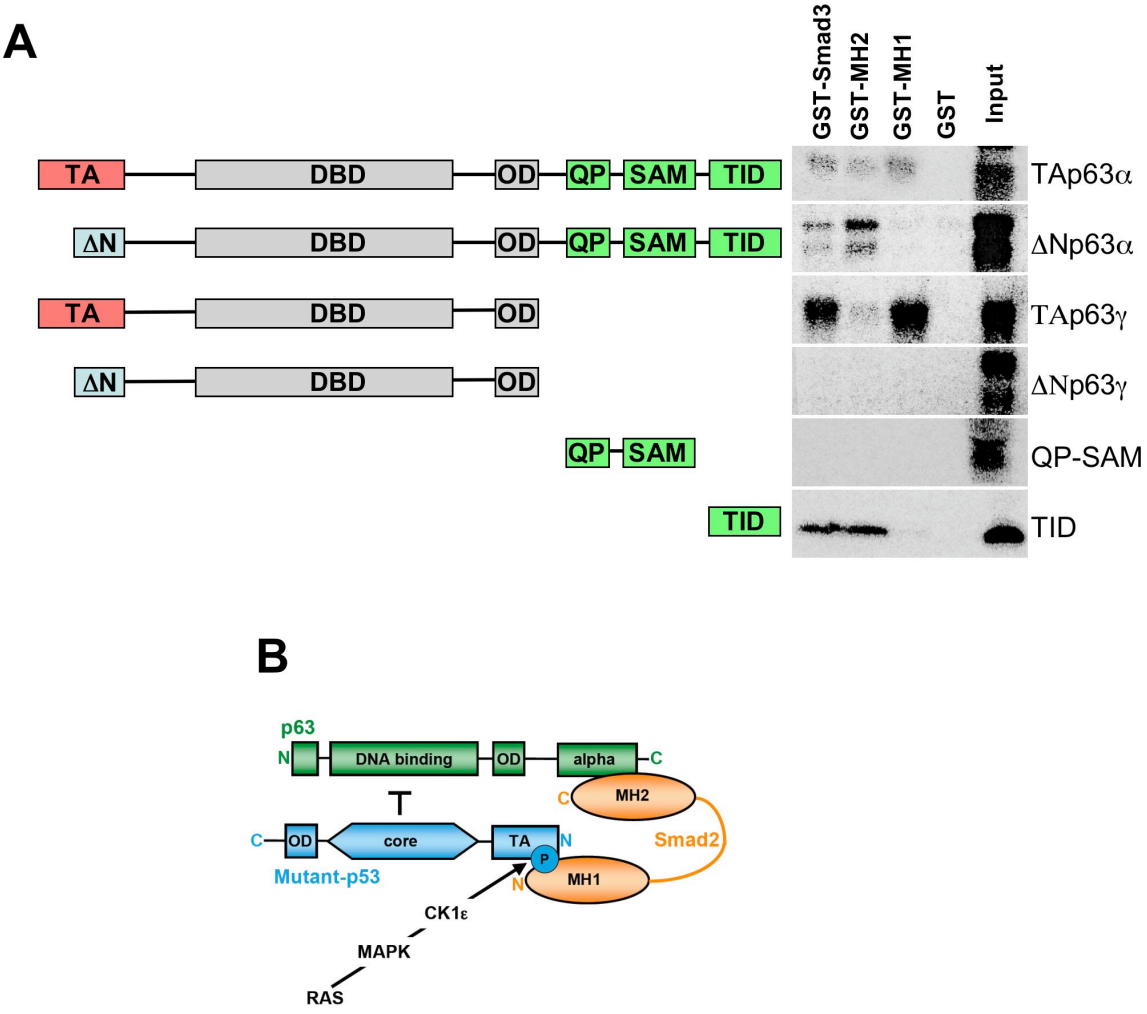
A
GST-Smad3
GST-MH2
GST-MH1
GST
Input
TA
DBD
OD
QP
SAM
TID
ΔN
TAp63α
ΔNp63α
TAp63γ
ΔNp63γ
QP-SAM
TID
B
p63
N
DNA binding
OD
alpha
C
MH2
T
C
OD
core
TA
N
P
Smad2
Mutant-p53
N
MH1
CK1ε
MAPK
RAS

Figure 7. Mechanism of p63 activity inhibition by mutant-p53 and TGFβ.

(C) Activation by p63 of the p53 reporter, p53BE-lux, is *per se* not affected by TGFβ stimulation. H1299 null cells were transiently transfected with the p53BE-lux reporter and increasing amount of p63 expression vectors.

(D) TGFβ signaling empowers the inhibition of p63 transcriptional activity by mutant-p53. H1299 null cells were transiently transfected with the p53BE-lux reporter and indicated p53/p63 expression vectors. Graphs show inhibition of the luciferase activity in cells cotransfected with p63 and a panel of mutant-p53 isoforms, coding for distincts hot-spot mutant-p53 alleles. Wild-type p53 is uneffective.

(E) ChIP analysis of p63 bound to its cognate responsive elements of the endogenous CDKN1A promoter and transfected recombinant p53-BE-lux. H1299 cells were transfected with p63, mutant-p53 or constitutive-active TGFβ receptor expression vectors (TGFβ), as indicated. IgG in lane 1 are irrelevant total rabbit immunoglobulins, used as background control. p63 western blotting ensures comparable pull-downs.

Figure 7

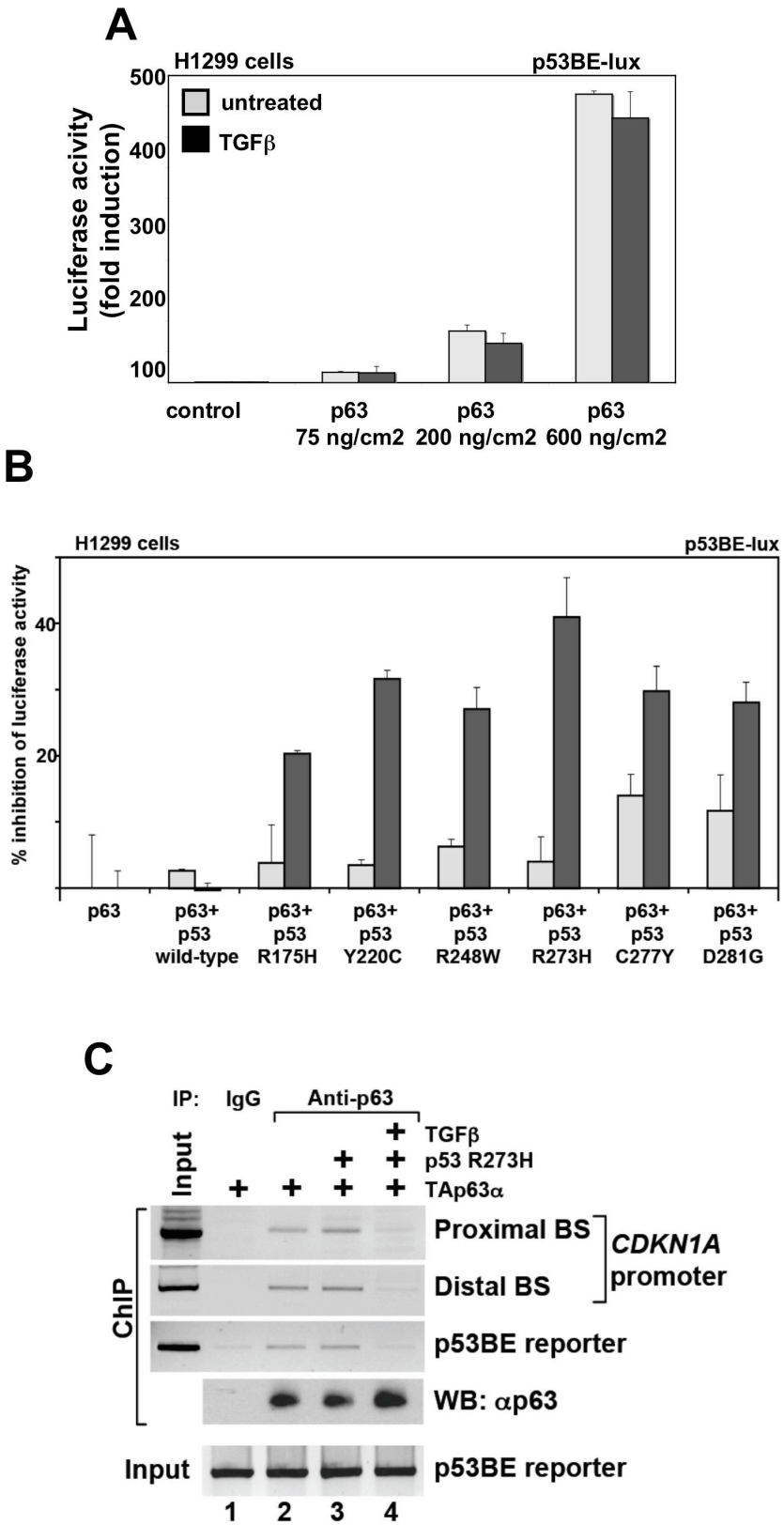
A
H1299 cells
p53BE-lux
untreated
TGFβ
Luciferase acivity (fold induction)
500
400
300
200
100
control
p63 75 ng/cm2
p63 200 ng/cm2
p63 600 ng/cm2
B
H1299 cells
p53BE-lux
% inhibition of luciferase activity
40
20
p63
p63+ p53 wild-type
p63+ p53 R175H
p63+ p53 Y220C
p63+ p53 R248W
p63+ p53 R273H
p63+ p53 C277Y
p63+ p53 D281G
C
IP: IgG
Anti-p63
Input
TGFβ
p53 R273H
TAp63α
ChIP
Proximal BS
Distal BS
CDKN1A promoter
p53BE reporter
WB: αp63
Input
p53BE reporter
1 2 3 4

Figure 8. p63 titration by mutant-p53 and Smad regulates metastasis

(A) Western blot analysis of spindle cells D3 and their metastatic derivative D3S2 cells for Smad2, p63 and mutant-p53. p63 is detected after immunoprecipitation.

(B) Coimmunoprecipitation of p63 with mutant-p53 from D3 and D3S2 cell lysates. Increases in TGFβ signaling parallels with increasing incorporation of free p63 into ternary complexes (lanes 1-3). Complex formation is disabled after Smad2/3 knockdown.

(C) To quantify the fraction of free-p63 in the D3 series, we immunoprecipitated mutant-p53 and then quantified associated p63 by western blot and finally compared this quantification to that one of the total p63 of the corresponding extract. The graph in the y-axis indicated the remaining free p63.

(D-E) Lung colonization assay of control and mutant-p53-, CK1δ/ε- and HRas-depleted D3S2 cells after tail vein injection in SCID mice (n=8-12 for each depleted cell population, 2 x 10^5 cells mouse). When injected subcutaneously, control and siRNA-depleted cell population displayed comparable growth-rates (not shown). (E) Panels show the corresponding immunoblotting.

(F) Expression of constitutive active Smad2 in D3 cells (D3S2 cells) induces metastatic ability (Oft et al., 2002). SCID mice were injected in the tail vein with D3 or D3S2 cells (n=8 for each cell lines, 2 x 10^5 cells/mouse); lung nodules were counted in H&E stained histological sections 24 days post-injection.

(G-I) D3S2 or D3S2-p63 cells were injected as in (D) (n=10 for each line, 2 x 10^5 cells/mouse).

(G) Number of metastatic nodules in the lungs.

(H and I) Representative haematoxylin and eosin staining of lung sections from mice injected with D3S2 and D3S2-p63 cells; M, metastatic nodule.

Figure 8

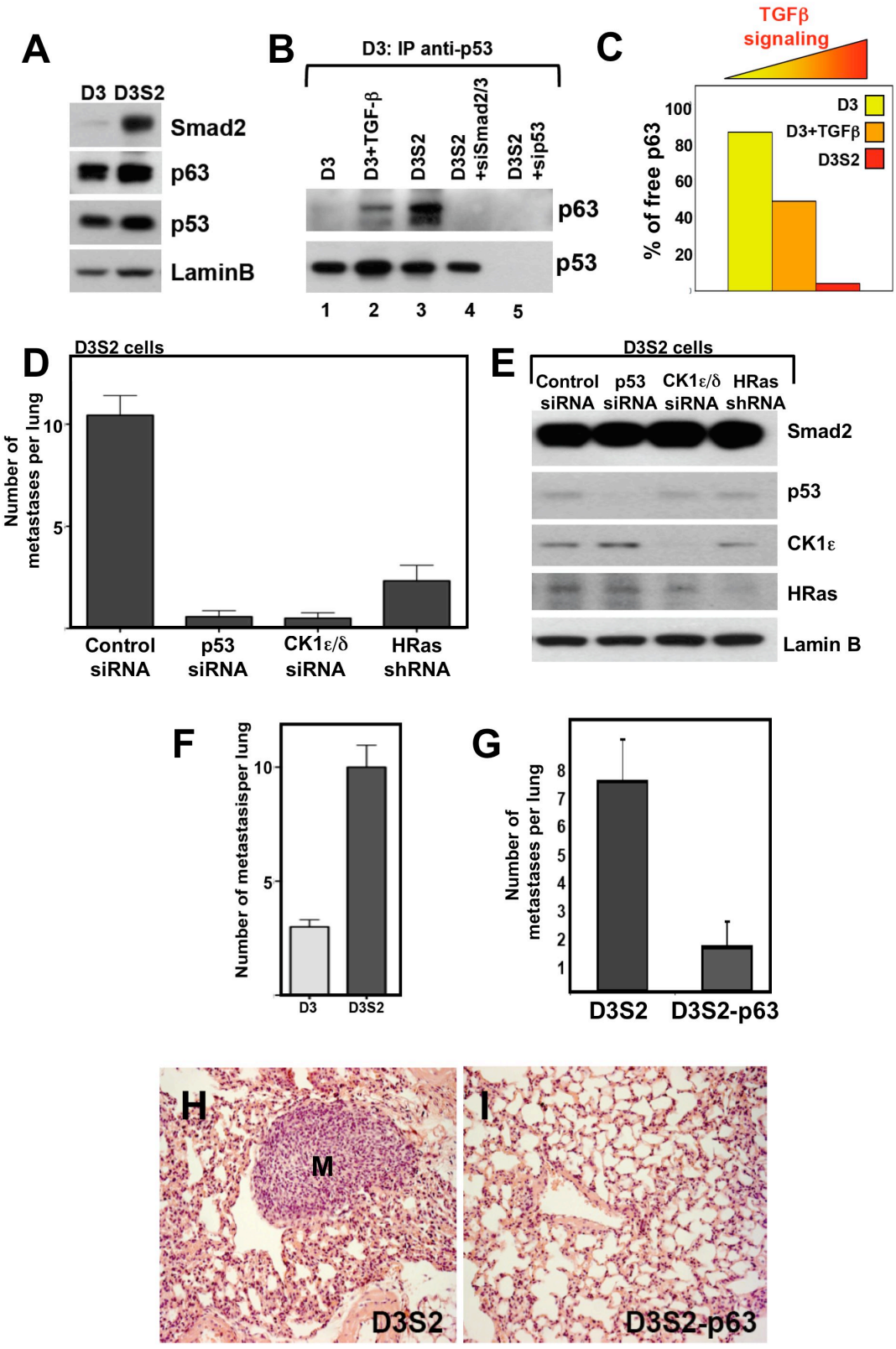
A
D3 D3S2
Smad2
p63
p53
LaminB
B
D3: IP anti-p53
D3
D3+TGF-β
D3S2
D3S2 +siSmad2/3
D3S2 +sip53
p63
p53
1 2 3 4 5
C
TGFβ signaling
% of free p63
100
80
60
40
20
D3
D3+TGFβ
D3S2
D
D3S2 cells
Number of metastases per lung
10
5
Control siRNA
p53 siRNA
CK1ε/δ siRNA
HRas shRNA
E
D3S2 cells
Control siRNA
p53 siRNA
CK1ε/δ siRNA
HRas shRNA
Smad2
p53
CK1ε
HRas
Lamin B
F
Number of metastasisper lung
10
5
D3
D3S2
G
Number of metastases per lung
8
7
6
5
4
3
2
1
D3S2
D3S2-p63
H
M
D3S2
I
D3S2-p63

Figure 9. Identification and clinical validation of a new class of candidate metastasis suppressors downstream of the TGFβ/mutant-p53/p63 axis.

(A) Overview of TGF_ target genes from microarray analysis of MDA-MB-231 cells. The graph shows functional classification for genes regulated by TGFβ in both MDA shGFP and MDA shp53 cell lines. Many genes codes for protein involved in cell invasion, migration and metastasis ("invasive program").

(B) Schematic representation of the dual role for TGFβ in promoting metastasis. TGFβ activates an invasive program independently of mutant-p53 expression. p63 restrains the deployment of this program by inducing metastasis suppressor genes. In mutant-p53 expressing cells, TGFβ can overcome this block by inactivating p63 through the mutant-p53/Smad2 axis.

(C) Sharp-1 and Cyclin G2 are targets of endogenous p63 in MDA-MB-231 cells. Graphs show Sharp-1 and Cyclin G2 mRNA expression monitored by Q-PCR from cells transfected with control or anti-p63 siRNAs.

(D) The impairment of TGFβ-driven migration of mutant-p53 depleted cells in transwell assays can be rescued by concomitant depletion of Sharp-1 or Cyclin G2.

(E) Northern blot validation of ADAMTS9, Sharp-1, Cyclin G2, Follistatin and GPR87 as mutant-p53 dependent target of TGFβ in MDA-MB-231. Where indicated, cells were treated for two hours with TGFβ1. GAPDH is a loading control.

Figure 9

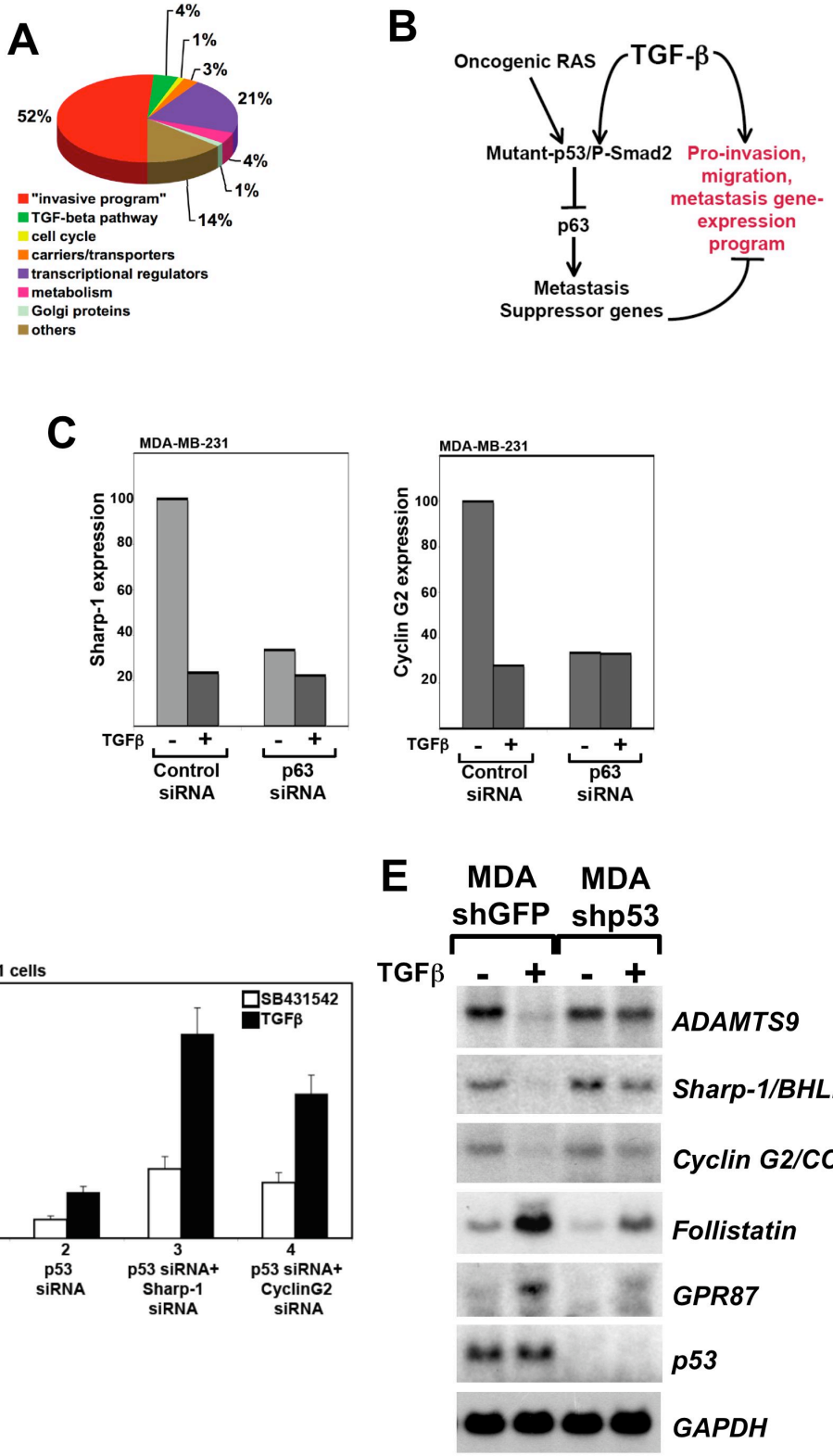
A
4%
1%
3%
21%
52%
4%
1%
14%
"invasive program"
TGF-beta pathway
cell cycle
carriers/transporters
transcriptional regulators
metabolism
Golgi proteins
others
B
Oncogenic RAS
TGF-β
Mutant-p53/P-Smad2
Pro-invasion, migration, metastasis gene-expression program
p63
Metastasis Suppressor genes
C
MDA-MB-231
Sharp-1 expression
100
80
60
40
20
TGFβ - + - +
Control siRNA
p63 siRNA
MDA-MB-231
Cyclin G2 expression
100
80
60
40
20
TGFβ - + - +
Control siRNA
p63 siRNA
D
MDA-MB-231 cells
migrated cells
1600
1400
1200
1000
800
600
400
200
0
SB431542
TGFβ
1 Control siRNA
2 p53 siRNA
3 p53 siRNA+ Sharp-1 siRNA
4 p53 siRNA+ CyclinG2 siRNA
E
MDA shGFP
MDA shp53
TGFβ - + - +
ADAMTS9
Sharp-1/BHLHB3
Cyclin G2/CCNG2
Follistatin
GPR87
p53
GAPDH

Figure 10. TGFβ–induced ternary complex inhibits p63 binding to metastasis suppressor gene's promoter.

ChIP analysis of endogenous p63 bound to its binding element in *Cyclin G2*. Lane 1 is a negative control ChIP carried out with aspecific rabbit IgG. Lower panel: Mapping a p63 binding site in Cyclin G2 (see methods).

Table1. Breast Cancer datasets analyzed for the clinical validation of the minimal signature.

Figure 10

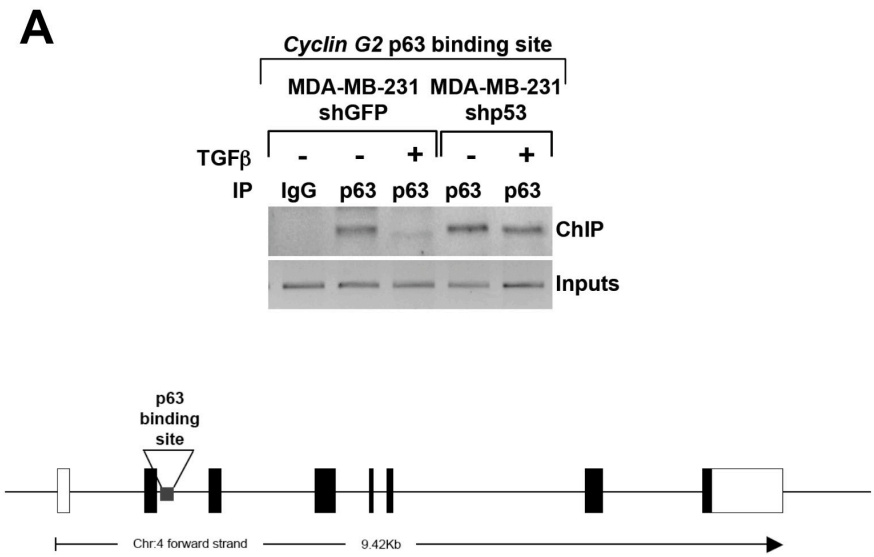

Table 1: Breast Cancer dataset analyzed in this study

Study	Microarray platform	Samples	Data source	Reference
Stockholm	Affymetrix HG-U133A	156	GEO GSE1456	Pawitan et al., 2005
NCI	Affymetrix HG-U133A	187	GEO GSE2990	Sotiriou et al., 2006
EMC	Affymetrix HG-U133A	286	GEO GSE2034	Wang et al., 2005
Uppsala	Affymetrix HG-U133A	236	GEO GSE3494	Miller et al., 2005
MSK	Affymetrix HG-U133	82	GEO GSE2603	Minn et al., 2005
NKI	Agilent, Rosetta Inpharmatics	295	http://www.rii.com/publications/2002/nejm.html; http://microarray-pubs.stanford.edu/wound_NKI/explore.html	van 't Veer et al., 2002; van de Vijver et al., 2002; Fan et al., 2006

Figure 11. Clinical validation of minimal signature.

(A-E) Analysis for the predictive role of the *minimal signature*. This analysis has been conducted on a panel of 5 independent Affymetrix-based datasets summing-up more than 940 tumors and Agilent-based NKI dataset (295 tumors). See Table 1 for a complete description of these data. Sharp-1 and Cyclin G2 expression values was used to separate tumor samples in two groups (see Experimental Procedures), with coherent low or high expression of both genes, as visualized by box-plots. 'Low' (blue) and 'High' (red) are the names of the *minimal signature Low* and *minimal signature High* groups, respectively. Kaplan-Meier graphs show the probability that patients, stratified according to the *minimal signature*, would remain free of metastases, free of recurrence, or free of disease in the analyzed breast cancer datasets. The p-value of the log-rank test reflects a significant association between *minimal signature High* and longer survival. Similar results were obtained using unsupervised clustering methods to generate the *minimal signature Low* and *minimal signature High* groups (data not shown). On the right, Kaplan-Meier survival graphs from the same tumor data stratified according to the 70 genes signature (van 't Veer et al., 2002).

Figure 11

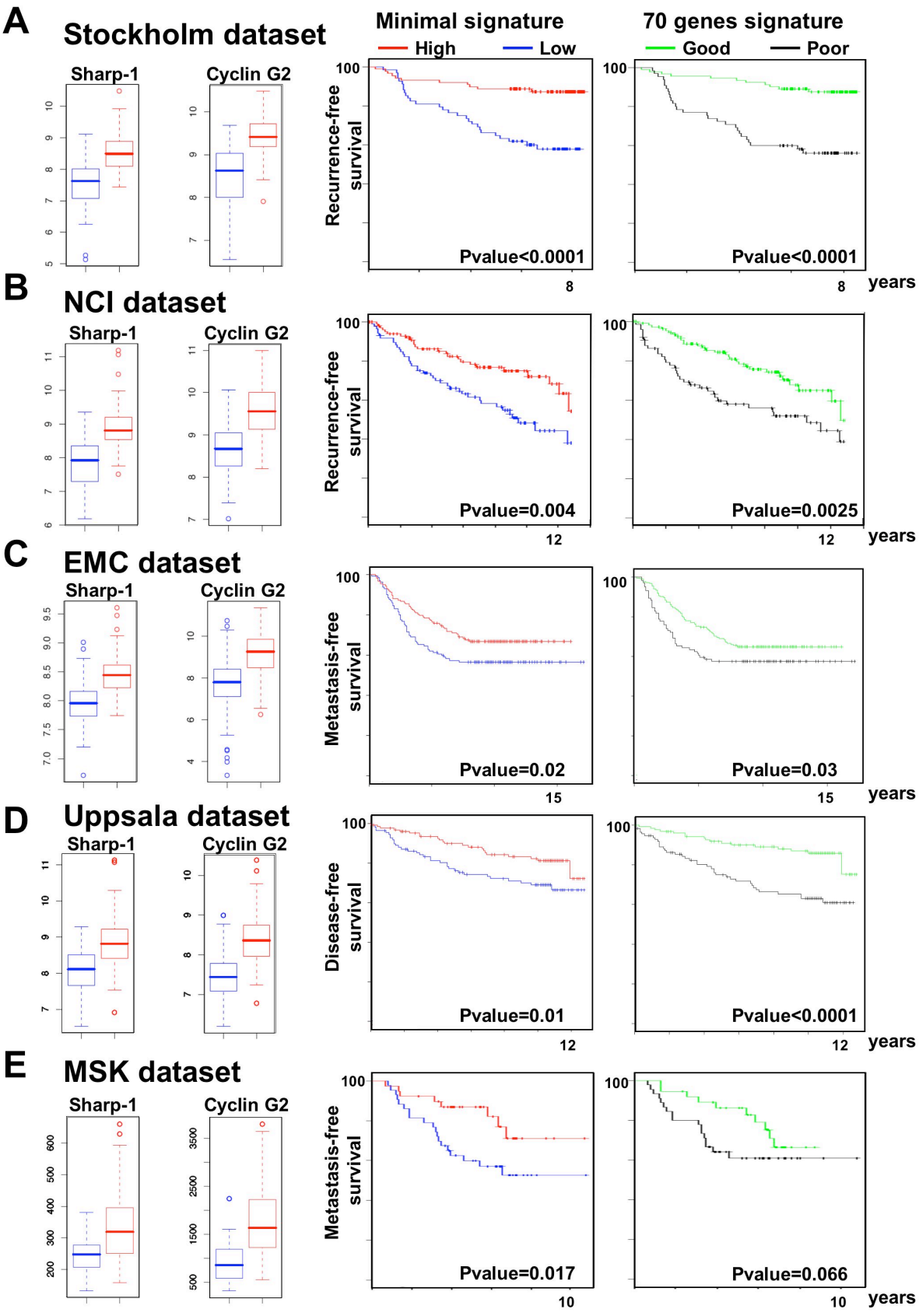
A
Stockholm dataset
Sharp-1
Cyclin G2
Minimal signature
High
Low
70 genes signature
Good
Poor
Recurrence-free survival
Pvalue<0.0001
Pvalue<0.0001
years
B
NCI dataset
Sharp-1
Cyclin G2
Recurrence-free survival
Pvalue=0.004
Pvalue=0.0025
years
C
EMC dataset
Sharp-1
Cyclin G2
Metastasis-free survival
Pvalue=0.02
Pvalue=0.03
years
D
Uppsala dataset
Sharp-1
Cyclin G2
Disease-free survival
Pvalue=0.01
Pvalue<0.0001
years
E
MSK dataset
Sharp-1
Cyclin G2
Metastasis-free survival
Pvalue=0.017
Pvalue=0.066
years

Figure 12. The minimal signature is predictive for both lung and bone metastasis risk.

(A) Kaplan-Meier curves show the probability to remain free of lung (left) and bone (right) metastasis for MSK samples (Minn et al., 2005) stratified according to the *minimal signature*. The *minimal signature* has a statistically significant predictive power for both organ-specific metastasis events.

Figure 12

A

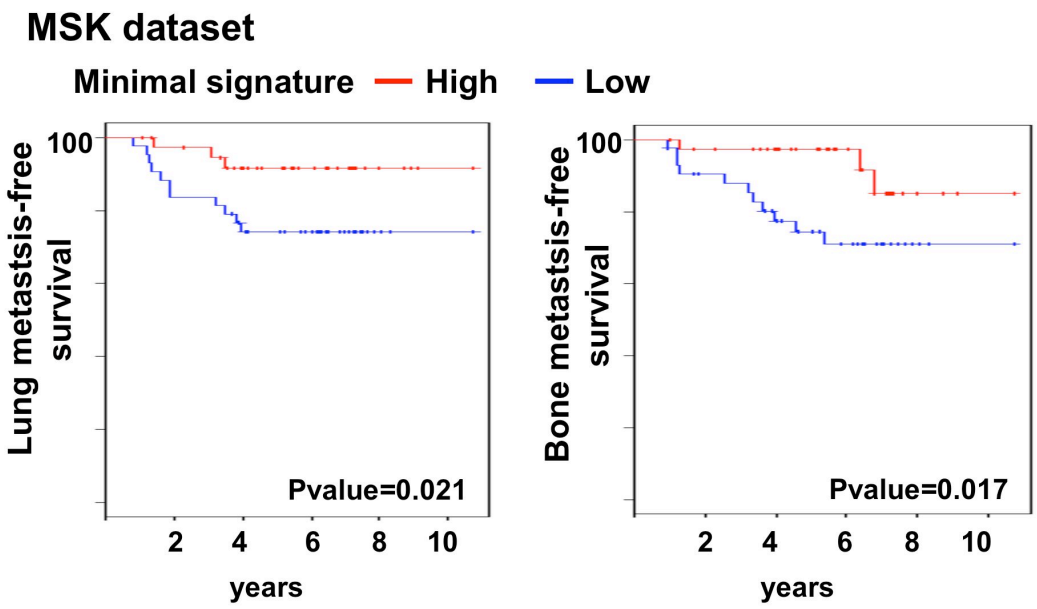
MSK dataset
Minimal signature
High
Low
Lung metastsis-free survival
100
Pvalue=0.021
2
4
6
8
10
years
Bone metastsis-free survival
100
Pvalue=0.017
2
4
6
8
10
years

Table 2: Multivariate analysis of risk of recurrence for the NCI dataset using a Cox proportional-hazard model

In Model 1, tumor size and grade 2 (versus grade 1) covariates have statistically significant coefficients at α=0.05. However, when the *minimal signature* is included (Model 2), affiliation to group 'Low', keeping constant all other covariates, significantly increases the hazard of recurrence by a factor of $e^{0.706}$=2.026 on average.

Model 1: Multivariate analysis using clinical variables only.

Model 1 was obtained using n=159 observations and its residual deviance (i.e., minus twice the partial log likelihood) is equal to 492.8774.

Variable	Hazard ratio	Hazard ratio 95% confidence interval	p-value
Tumor diameter > 2 cm (<= 2cm)	2.206	(1.242 - 3.92)	0.0069
Node positive (vs. node negative)	0.815	(0.304 - 2.19)	0.6900
Grade 2 (vs. Grade 1)	2.327	(1.037 - 5.22)	0.0410
Grade 3 (vs. Grade 1)	1.282	(0.597 - 2.75)	0.5200
ER positive (vs. ER negative)	0.790	(0.414 - 1.50)	0.4700
Tamoxifen treatment	1.564	(0.645- 3.79)	0.3200

Model 2: Multivariate analysis using clinical variables and the *minimal signature*.

Model 2 was obtained using n=159 observations and its residual deviance (i.e., minus twice the partial log likelihood) is equal to 486.8369.

Variable	Hazard ratio	Hazard ratio 95% confidence interval	p-value
Tumor size (cm)	2.198	(1.228 - 3.94)	0.008
Node positive (vs. node negative)	0.787	(0.294 - 2.11)	0.630
Grade 2 (vs. Grade 1)	2.084	(0.927 - 4.68)	0.076
Grade 3 (vs. Grade 1)	0.973	(0.437 - 2.17)	0.950
ER positive (vs. ER negative)	0.818	(0.427 - 1.57)	0.540
Tamoxifen treatment	1.504	(0.618 - 3.66)	0.370
Group Low (vs. Group High)	2.026	(1.141 - 3.60)	0.016

Model 1 and Model 2 may be compared to assess whether the *minimal signature* adds additional prognostic information over the clinical variables. In particular, the value of adding the *minimal signature* to Model 1 is obtained by subtracting the residual deviance of Model 1 from the one of Model 2 and testing this difference against a chi-square distribution with one degree of freedom. The difference between the residual deviances of the model constructed without the *minimal signature* (i.e., Model 1) and the model including the *minimal signature* (i.e., Model 2) is equal to 492.8774 – 486.8369 = 6.04043 and exceeds the .95 quantile of the chi-square distribution with one degree of freedom (p-value = 0.01398). As such, the *minimal signature* is a significant predictor of recurrence-free survival, adding new prognostic information beyond the one provided by the standard clinical predictors. In addition, the minimal signature adds prognostic value not only to the multivariate model but also to any model constructed using any single clinical predictor. Indeed, the difference between the residual deviance of the model obtained using a single clinical variable plus the *minimal signature* (e.g., tumor diameter+*minimal signature*) and the residual deviance of the model obtained using only a clinical variable, is significant for each clinical predictor.

Clinical predictor	Difference of residual deviances	p-value
Tumor size	4.3611	0.0368
Nodal status	7.4596	0.0063
Tumor grade	5.6859	0.0171
ER status	6.6992	0.0096
Treatment status	6.772	0.0093

Figure 13. Minimal signature add prognostic information to estabilished clinical predictors.

(A) The minimal signature is an independent predictor of recurrence-free survival for breast cancer adding additional prognostic information over size, node status, histological grade, ER status and age. This analysis was conducted on the NKI dataset, listing 295 tumors (Fan et al., 2006). Graphs are Kaplan-Meier curves showing the probability of remaining disease-free for patients stratified according the indicated established clinical predictors (panels on the left). On the right, each category of tumors were further split in two groups by applying the *minimal signature* (red line: *minimal signature* high; blue line: *minimal signature* low). Note how combining the minimal signature with individual clinical predictors significantly improves patients' stratification. For example, in the case of size, patients can be now split in groups with increased probability of survival (size>2cm + "low"; size<2cm + "low"; size>2cm + "high"; size<2cm + "high").

A

Figure 13

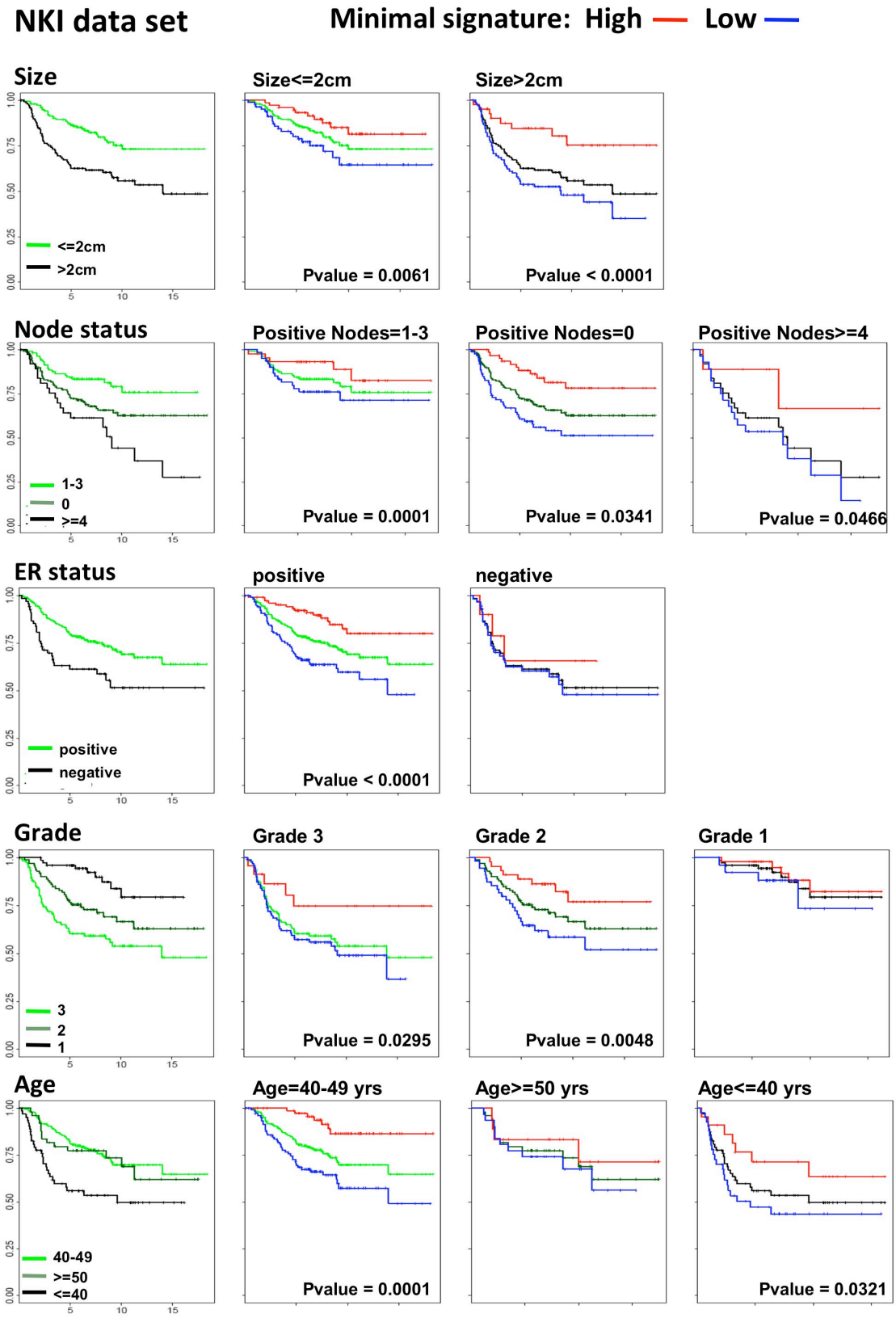
NKI data set
Minimal signature: High Low
Size
<=2cm
>2cm
Size<=2cm
Pvalue = 0.0061
Size>2cm
Pvalue < 0.0001
Node status
1-3
0
>=4
Positive Nodes=1-3
Pvalue = 0.0001
Positive Nodes=0
Pvalue = 0.0341
Positive Nodes>=4
Pvalue = 0.0466
ER status
positive
negative
positive
Pvalue < 0.0001
negative
Grade
3
2
1
Grade 3
Pvalue = 0.0295
Grade 2
Pvalue = 0.0048
Grade 1
Age
40-49
>=50
<=40
Age=40-49 yrs
Pvalue = 0.0001
Age>=50 yrs
Age<=40 yrs
Pvalue = 0.0321

Figure 14. The minimal signature is an independent predictor of recurrence-free survival for breast cancer over estabilished breast cancer treatments.

(A) The minimal signature is an independent predictor of recurrence-free survival for breast cancer over chemotherapy, hormonal therapy and mastectomy. These analyses were conducted on the NKI dataset.

Figure 14

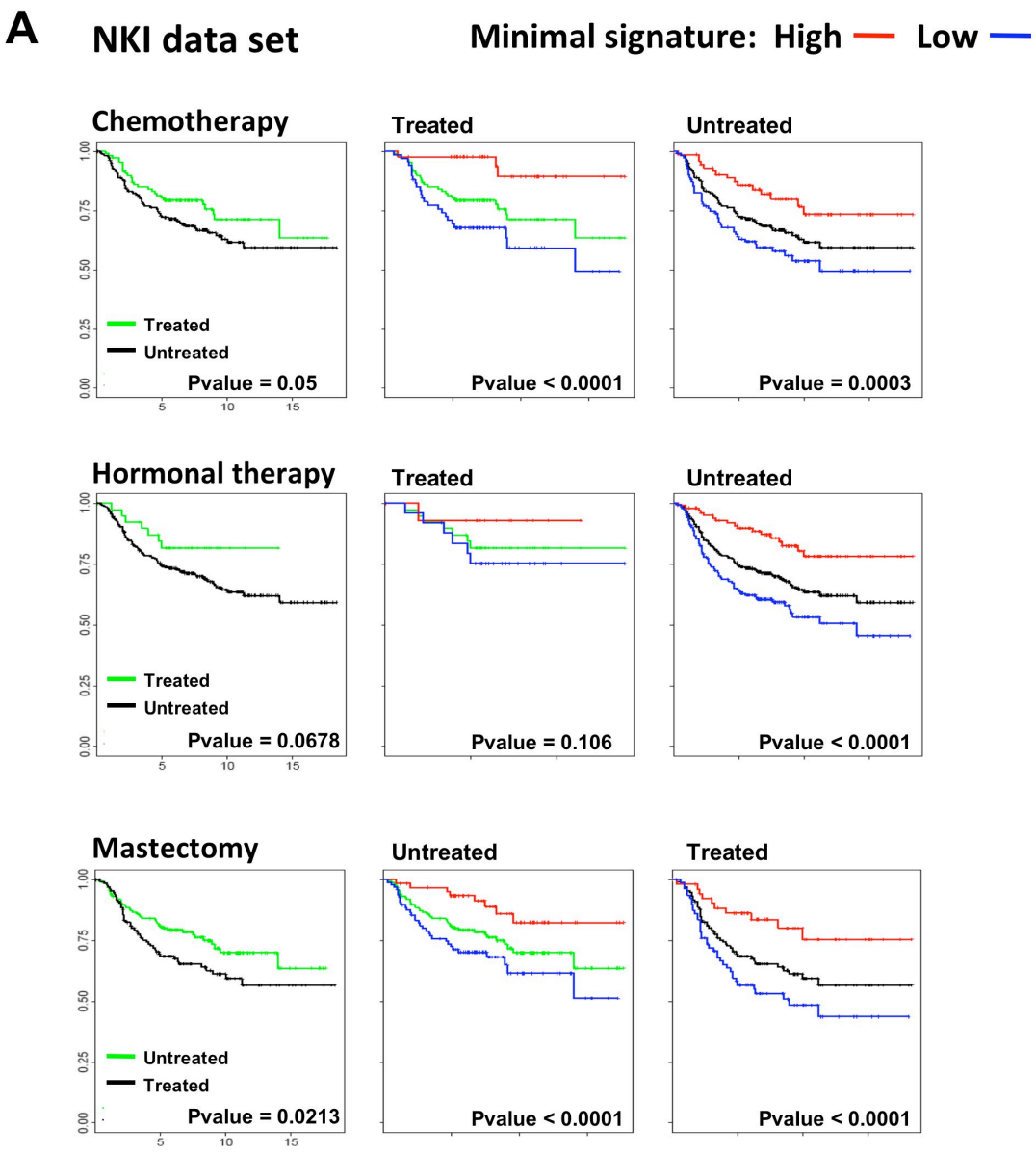
A
NKI data set
Minimal signature: High Low
Chemotherapy
Treated
Untreated
Pvalue = 0.05
Treated
Pvalue < 0.0001
Untreated
Pvalue = 0.0003
Hormonal therapy
Treated
Untreated
Pvalue = 0.0678
Treated
Pvalue = 0.106
Untreated
Pvalue < 0.0001
Mastectomy
Untreated
Treated
Pvalue = 0.0213
Untreated
Pvalue < 0.0001
Treated
Pvalue < 0.0001

Figure 15. The minimal signature identifies subgroups with different prognosis in populations of patients defined as "intermediate" by known clinical predictors.

(A) Kaplan-Meier curves showing the probability of remaining free of recurrence, disease or metastasis for patients from the Stockholm, Uppsala and NKI datasets stratified according the Nottingham histological scale (grade 1 dotted line; grade 2, violet line; and grade 3, dashed line). Grade 2 tumors were further split in two groups by applying the *minimal signature* (red line: grade 2 and *minimal signature* high; blue line: grade2 and *minimal signature* low). Notably, the high and low groups displayed a recurrence-free survival rate similar to the grade 1 or grade 3 patients, respectively.

Figure 15

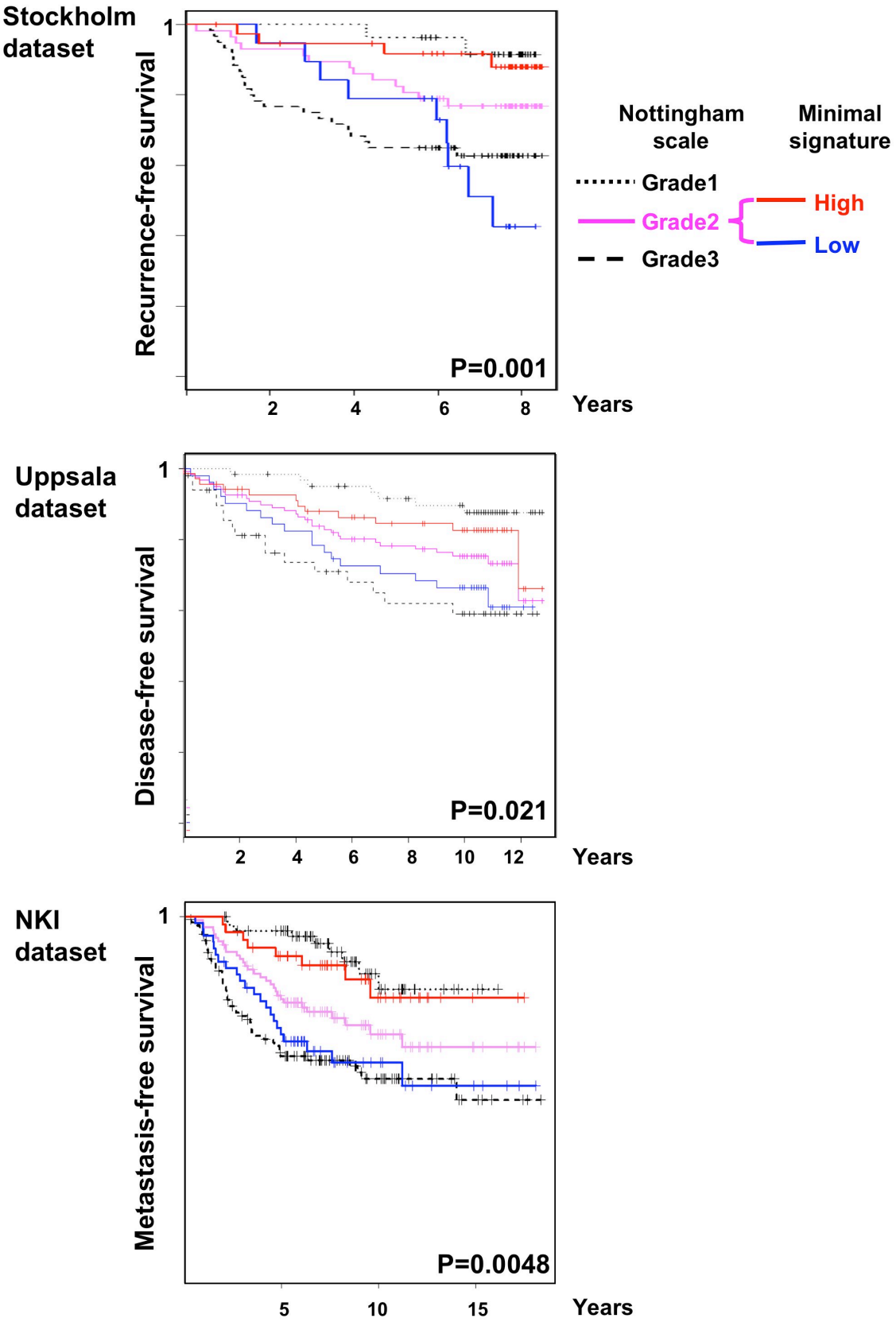
Stockholm dataset
Recurrence-free survival
1
2
4
6
8
P=0.001
Years
Nottingham scale
Minimal signature
Grade1
Grade2
Grade3
High
Low
Uppsala dataset
Disease-free survival
1
2
4
6
8
10
12
P=0.021
Years
NKI dataset
Metastasis-free survival
1
5
10
15
P=0.0048
Years

Supplemental Table S1

Target Gene	Name	Sequence (sense)	Species	References
GFP	shGFP	CAAGCTGACCCTGAAGTTC	-	-
p53	p53 siRNA A, p53 siRNA	CCGCGCCATGGCCATCTACA	Human and mouse	Cordenonsi et al., 2003
p53	p53 siRNA B, shp53	GACTCCAGTGGTAATCTAC	Human	-
Smad4	shSMAD4	GGTGTGCAGTTGGAATGTA	Human	Padua et al., 2008
Smad4	Smad4 siRNA	GTACTTCATACCATGCCGA	Human	Dupont et al., 2005
Human p63	p63 siRNA A, p63 siRNA	CGACAGTCTTGTACAATTT	Human	Dharmacon siGenome
Human p63	p63 siRNA B	CGACAGTCTTGUACAATTT	Human	Dharmacon siGenome
Mouse p63	p63 siRNA	ATGAAATTGTACAGGACTG	Mouse	Nguyen et al., 2006
Smad2	Smad2 siRNA	GCTTAGGTTTACTCTCCAATG TTAA	Human and Mouse	Invitrogen-stealth
Smad3	Smad3 siRNA	GATGCAACCTGAAGATCTTCA ACAA	Human and Mouse	Invitrogen-stealth
CK1ε and CK1δ	CK1ε/δ siRNA	TGGCCAAGAAGTACCGGGA	Human and Mouse	Liu et al., 2002
HRas	shHRas	ACAGGTGGTCATTGATGGG	Mouse	Rubin et al., 2005
Sharp-1	Sharp-1 siRNA A	GCTTTAACCGCCTTAACCG	Human	-
Sharp-1	Sharp-1 siRNA B	CGAGACGACACCAAGGATA	Human	-
Cyclin G2	Cyclin G2 siRNA A	GAGTCGGCAGTTGCAAGCT	Human	-
Cyclin G2	Cyclin G2 siRNA B	AGAATACTCGGCTAGGCAT	Human	-
Scramble	Control siRNA	TTCTCCGAACGTGTCACGT	-	Dupont et al., 2005

Supplemental Table S2

RT-PCR primers	
Name	**Sequence**
Actin for	ATGAAGTGTGACGTTGACATCCG
Actin rev	GCTTGCTGATCCACATCTGCTG
p53 for	CTGGCCCCTGTCATCTTCTGTC
p53 rev	CACGCAAATTTCCTTCCACTCG
p63 for	GCCACCTGGACGTATTCCACTG
p63 rev	TAAAATTGGACGGCGGTTCATC
SHARP-1 for	GCATGAAACGAGACGACACC
SHARP-1 rev	CGCTCCCCATTCTGTAAAGC
Cyclin G2 for	CCTCCCAGTGATCAAGAGTGC
Cyclin G2 rev	TCCCTCCTCCCCAAAGTAGC

Q-PCR primers	
Name	**Sequence**
GAPDH for	AGCCACATCGCTCAGACAC
GAPDH rev	GCCCAATACGACCAAATCC
SHARP-1 for	CGTCTTTGGAGTTGACATGG
SHARP-1 rev	GGGCAGCTTTGAGAACTAGC
Cyclin G2 for	TGGACAGGTTCTTGGCTCTT
Cyclin G2 rev	GATGGAATATTGCAGTCTTCTTCA

ChIP primers	
Name	**Sequence**
CDKN1A distal for	TCCTCCTTCTTCAGGCTTGG
CDKN1A distal rev	TGCTGGCAGATCACATACCC
CDKN1A proximal for	GGGGGTCTGCTACTGTGTCC
CDKN1A proximal rev	GACCTCCCCTGGACTTCACC
Mix.2 p53BE for	CGAGCTCTTACGCGTGCTA
Mix.2 p53BE rev	GGGCTGAACCGGGCAATGA
Cyclin G2 p63BS for	AGGGCTGAGTTTGATTGAGG
Cyclin G2 p63BS rev	AGCTGCAGGCTGGAGTATGG